Universidad del País Vasco
Euskal Herriko Unibertsitatea

KIMIKA FAKULTATEA
FACULTAD DE QUÍMICA

Universidad del País Vasco/Euskal Herriko Unibertsitatea

Facultad de Química/Kimika Fakultatea

Grado en Química

TRABAJO FIN DE GRADO

3D Printing of Virgin PET. Effect of processing parameters.

Autora: Zoi Ganosi Uribezubia

Dirigido por: Itxaso Calafel Martinez & Alejandro J. Müller

San Sebastián, septiembre de 2021

GIPUZKOAKO CAMPUSA
CAMPUS DE GIPUZKOA
Pº. Manuel de Lardizabal, 3
20018 DONOSTIA-SAN SEBASTIAN
GIPUZKOA

3D PRINTING OF VIRGIN PET. EFFECT OF PROCESSING PARAMETERS.

Zoi Ganosi Uribezubia

UPV/EHU

ABSTRACT

The use of filaments made of recycled materials such as PET on fused deposition modelling (FDM) is aspired to be one of the innovative techniques for sustainable and environmentally friendly production. However, to carry out such a development, it is crucial to understand the behaviour of virgin PET and optimise the printing parameters to obtain the best results. Research of the effect that FDM technology can have on the mechanical properties of 3D-printed products made of polyethylene terephthalate (PET) filaments has been carried out. The bed temperature of the printer is one of the most important parameters to be controlled since by increasing the temperature from 70 ºC to 100 ºC, the polymer crystallizes (cold crystallization) and the fragility of the specimens is increased. The same observation happens with injected specimens by increasing the mould temperature from 25 ºC to 85 ºC, where the ductility of the specimen decreases. Using differential scanning calorimetry, the crystallinity degree of each specimen was measured. Through a scanning electron microscope, the printing parameters influence on the quality of structure and filament adhesion were observed. Optimization of process parameters is required to obtain amorphous specimens that can reach the mechanical performance of injected PET specimens.

RESUMEN

El uso de filamentos elaborados con materiales reciclados como el PET en la tecnología de impresión 3D, aspira ser una de las técnicas innovadoras para una producción sostenible y ambientalmente favorable. Sin embargo, para llevar a cabo tal desarrollo es imprescindible conocer el comportamiento del PET virgen, así como los parámetros de procesado que permitan obtener las mejores prestaciones de este material. El trabajo se centra en la

investigación del efecto que la tecnología FDM tiene en las propiedades mecánicas de productos hechos con filamento de polietilén tereftalato (PET). La temperatura de la cama de la impresora es de los parámetros más importantes para controlar ya que al subir la temperatura de 70 ºC a 100 ºC, el producto cristaliza (cristalización en frío) y la fragilidad de las probetas aumenta. Lo mismo ocurre en el caso de probetas inyectadas al subir la temperatura del molde de 25 ºC a 85ºC, donde la ductilidad de las probetas decrece. Aplicando la calorimetría diferencial de barrido, se ha determinado el grado de cristalinidad, encontrándose un gradiente de cristalinidad en el espesor de la probeta. Con la microscopia electrónica de barrido se ha observado la influencia que tienen la temperatura y el patrón de impresión en la calidad de la misma. Se requiere la optimización de los parámetros de procesado en impresión 3D para obtener probetas amorfas que se acerquen a la resistencia mecánica de las probetas de PET inyectadas.

Table of Contents

Table of Figures

ABBREVIATIONS

ABS: Acrylonitrile Butadiene Styrene

AM: Additive Manufacturing

ASTM: American Society for Testing and Material

DMTA: Dynamic Mechanical Thermal Analysis

DSC: Differential Scanning Calorimetry

FDM: Fused Deposition Modelling

FFF: Fused Filament Fabrication

G´: Storage Modulus

G´´: Loss Modulus

HDPE: High-density Polyethylene

ISO: International Organization for Standardization

PBS: Polybutylene Succinate

PET: Polyethylene terephthalate

PLA: Polylactic acid

PP: Polypropylene

SEM: Scanning Electronic Microscope

SLS: Selective Laser Sintering

tan δ: Damping factor

T_g: Glass transition Temperature

X_c: degree of crystallinity

ΔH_m: melting enthalpy

ΔH_m^o: melting enthalpy of 100% crystalline polymer

ΔH_{cc}: enthalpy of cold crystallization

I. INTRODUCTION

I.i Environmental pollution

Despite the environmental and sustainability concerns, the production of plastics is constantly increasing. Due to their ease of manufacture, low cost, and other unique properties, plastics have replaced and displaced many other traditional materials. Given this versatility, it is not surprising that the demand for plastics is constantly rising. The last detailed report (2018) on the annual production of plastics for packaging purposes in Spain, showed it to exceed 1.655.189 tonnes. Although, the recycling rates are about 50%. Most of the unrecycled fraction ends up in the oceans, where it may be ingested and absorbed by the marine flora and fauna, altering ecosystems, and sooner or later, human health [1].

One of the problems that the recycling industry faces is the need for sorting different types of plastic. Furthermore, many commercial packaging contains more than one type of plastic, such as milk bottles with polyethylene terephthalate (PET) bodies and polypropylene (PP) lids. More efficient reprocessing techniques and innovative ways of recycling need to be developed. For instance, the possibility of elaborating filaments made of polymer blends of recycled materials for three-dimensional printing technologies could be a breakthrough for the recycling industry. Reusing mixed waste lowers the recycling cost and facilitates the tailoring of the mechanical properties of the final products by combining certain characteristics of the used polymers [2].

I.ii European Union and polymers

As mentioned above, the FDM printers could contribute to waste management by applying recycled plastic waste in filament elaboration[3,4]. Several recycled polymers have been employed for single component thermoplastic filaments, such as polylactic acid (PLA), high-density polyethylene (HDPE), acrylonitrile butadiene styrene (ABS) as well as composites (waste wood). Nevertheless, polyethylene terephthalate (PET) is one of the main recycled materials. A major percentage of beverage bottles are made of PET. This is due to this polyester´s unique properties such as high strength, chemical intolerance, and low production

cost. According to the European report (2017), the production of PET in the EU was around 4.45 million tonnes, figure 1 [5].

	PERIODO (año)	PRODUCCIÓN (millones de toneladas)	FUENTE
Producción mundial de plástico	2018	359	PlasticsEurope, 2019
Producción en la UE de plástico	2018	61,8	PlasticsEurope, 2019
Producción mundial de plástico PET	2017	30,3	Plastics Insight, s.f.
Producción en la UE de plástico PET	2017	4,45	Plastics Insight, s.f.
Generación acumulada de plásticos primarios y secundarios (reciclados)	1950-2015	6.300	Geyer et al., 2017

Figure 1: Plastic production in the world and the UE, expressed in millions of tones. Adapted from reference (11).

To tackle the ecological crises due to plastic pollution and marine litter, in 2018, the EU established new legislation for accelerating the transition to a circular plastics economy. By 2024, the recycled content in packaging is meant to be about 25%, while from 2030, PET bottles will have to contain at least 30% recycled plastic [6]. In addition, the European Commission ensures that all plastic packaging placed on the EU market is either reusable or easily recyclable. By pursuing these aims, the European Commission´s strategy will make a tangible contribution to reaching the 2030 Sustainable Development Goals[7,8]. It is therefore of utmost importance to concentrate efforts on the search for new processing methods and applications of materials containing recycled components.

I.iii PET overview

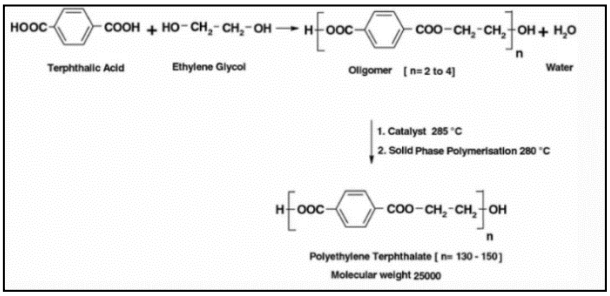

Figure 2: Polyethylene terephthalate synthesis. Adapted from reference (15)

PET is a synthesized thermoplastic polymer, which was patented by DuPont, and currently represents 50% of the fabric industry [9]. PET is a polyester formed from a polymeric reaction of condensation between terephthalic acid and ethylene glycol as shown in figure 2. PET is classified as a semi-crystalline polymer. Depending on the presence of additives and heat treatment, its crystallinity can be changed. If the amorphous polymer is heated approximately above 70 ºC, its structure changes from a rigid glass state into a viscous state in which the polymer chains are able to move and be oriented. In the case of packaging and film production, the chemical nature of PET is modified by adding some co-monomers that control its crystallinity.

I.iv PET Recycling

Since waste disposal affects the environmental equilibrium and PET is widely used in the beverage industry, and for packaging, researches about its recycling process and reuse are numerous. Fortunately, effective recycling mechanisms have been developed for PET. The first attempt of recycling a bottle made out of PET took place in 1977. Depending on the price of virgin PET, in figure 3, innovative and economically efficient recycling technologies are adopted by the recycling industry [10,11]. The main mechanism that is applied in this recycling process involves washing and remelting it to apply it to products that use PET as a component. This method is a part of mechanical recycling during which the basic polymer is not altered. On the other hand, chemical recycling can be applied too. In this case, PET is decomposed into its raw materials[9]. However, this method comes with the disadvantage of deteriorating

the product in every recycling process. Despite this disadvantage, recycled plastic products require 50-60% less energy than those with virgin resin [12].

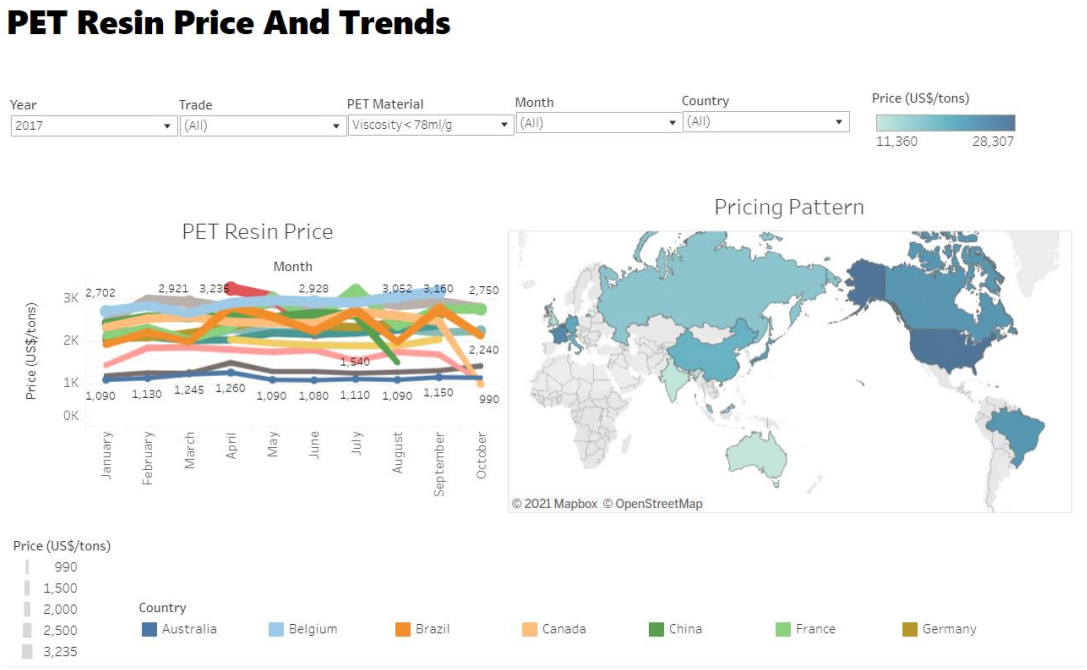

Figure 3: PET resin price trend depending on the country of production for 2017. Adapted from reference (4).

I.v 3D printing and polymers

The arrival of new technologies such as three-dimensional printing aspires to contribute to the solution of waste management[13]. Additive manufacturing (AM) presents a wide range of advantages over traditional manufacturing processes. Generally, in layer-by-layer manufacturing, there is no limitation in product design, and it is an automated process that allows higher design complexity and multiple material elaboration. Furthermore, it is a fast and inexpensive technique for requiring less energy and shorter cycle times [14]. Innovators can easily produce prototypes of their ideas as 3D printing greatly simplifies prototype production[15].

The first 3D printer based on the stereolithographic (SLS) technique was invented and commercialized by Charles Hull in 1986. However, nowadays, one of the most popular AM technologies is fused deposition modelling (FDM), also referred to as fused filament fabrication (FFF). The fundamental extrusion process technology was patented by Stratasys Corporation in 1989. Their first FDM machine was marketed in 1992 by the name 3D Modeler. Nowadays, FDM 3D printers are pretty common and can be found in various sizes and build volumes.[16].

I.vii FDM Technology

FDM technology is based on extruding fused filament made of polymers through a heated print nozzle that moves in two directions onto the printer's plate, layer by layer. Normally, a computer program is used to design the desired 3D object and give the G-code instructions. A schematic diagram of the FFF process is illustrated in figure 4. The extruder and nozzle of the printer are constantly fed with filament. Depending on the type of polymer that the filament has been elaborated on, the temperature of the nozzle will differ. Once the filament has melted, the material is deposited on the printer's bed until the final product is achieved. The bed temperature, the printing velocity, and the layer height are some of the main parameters that need to be configured for the printing process[3,17]. Once the printing process has ended, the printed components are removed by snapping off. Then, the printed object may need to be cleaned, painted, or get its support features to be removed[14].

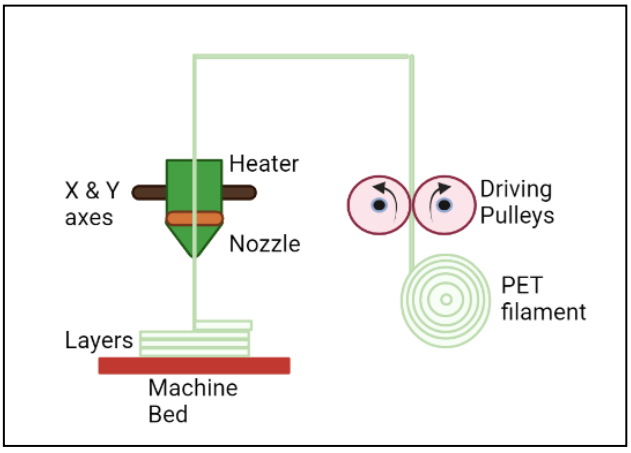

Figure 4: FDM technique and its main components

The aforementioned FDM advantages are several. However, the process contains some limitations. The surface finish and accuracy may not be as expected since the filament material is extruded through a circular nozzle. In addition, the layer-by-layer deposition process can cause a grainy surface finish due to the staircase effect where the layer marks become distinctly visible on the surface of the printed product. Moreover, there is a need for raw material staple filaments. Since such technology requires filaments with a specific diameter, the rheological and mechanical properties of new material have to be studied to transform it into a filament. From all the existing limitations, the most important one is the anisotropic properties that describe the final product. Since the parts are built layer by layer by depositing extruded rods, the mechanical properties vary in each direction. The majority of researches mention the influence of FDM process parameters on the mechanical properties of ABS, but very few focus on other polymers[3].

I.viii FDM technology and mechanical properties

In additive manufacturing techniques, it is crucial to properly select the process conditions in order to be a successful alternative way of FDM manufacturing. Indeed, this technique is a complex process that contains various parameters that can affect the mechanical properties and the quality of the final specimens [18,19]. Especially the process parameters such as nozzle temperature, bed temperature, printing flow, layer thickness, and specimen orientation have been found directly linked with the mechanical performance [13]. Piece quality, precise dimensions, waste avoidance, and production time are some of the aspects to be ensured. Figure 5 shows some of the parameters that have been studied to optimize the FDM process. Unfortunately, although there are numerous investigations about the effect of process parameters on the mechanical properties of 3D ABS, PBS and PLA parts, little is known about virgin PET or the mechanical behaviour of recycled PET[20]. It is therefore of vital importance to initially study the 3D behaviour of virgin PET to tackle the processability of recycled PET.

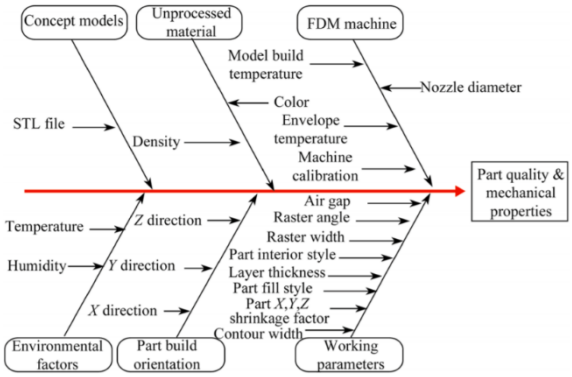

Figure 5: Cause and effect diagram of FDM process parameters. Adapted from reference (18).

II. AIMS

This study aims to present the optimal printing conditions with virgin PET to achieve mechanical properties close to the standards of injected PET specimens. The effect of main process parameters, namely nozzle temperature, bed temperature, printing velocity, and raster orientation, on Young´s modulus and deformation at break has been taken into consideration.

To achieve the relation between the mechanical properties and the printing parameters, a table of seven different combinations of variables has to be made. Furthermore, for the specimens of each combination, a tensile test has been carried out.

Differential scanning calorimetry (DSC), dynamic mechanical thermal analysis (DMTA) have been carried out to characterise the thermal properties of different specimens, as well as other polymer properties such as crystallinity degree to explain the resulting fluctuations between the mechanical properties.

Scanning electron microscopy (SEM) imaging will provide an insight into the internal structure (adhesion between layers) of the studied conditions.

On the other hand, injected specimens have been obtained at three different mould conditions, same as the printer´s bed temperature, to compare the mechanical properties of these with those obtained by 3D and to discuss the best 3D processing conditions.

III. EXPERIMENTAL

III.i Materials

A commercial polyethylene terephthalate (PET) resin was used to carry out this study. To be precise, the PET resin used was Novapet CR grade, with an intrinsic viscosity of 0.80 dl/g, provided by Brilen SA. The PET was supplied in pellets form, so the first step is to transform it into a filament with a suitable and homogeneous diameter to be used in 3D printing.

III.ii Elaboration of filaments

PET is a hygroscopic material, so drying is a mandatory requirement. For that reason, it was dried for 48h at 70 ºC with a dehumidifier.[2,21] Once dried, the Collin Teach-line ZK-25 twin-screw co-rotating extruder (25mm diameters with L/D relationship of 18:1) was used. The screw rotational speed and the nozzle temperature were fixed at 80 rpm and 271 ºC, respectively. Furthermore, the produced filament was cooled down with a water bath at room temperature, figure 6. The diameter of the obtained filament was between 1.60-1.75 mm.

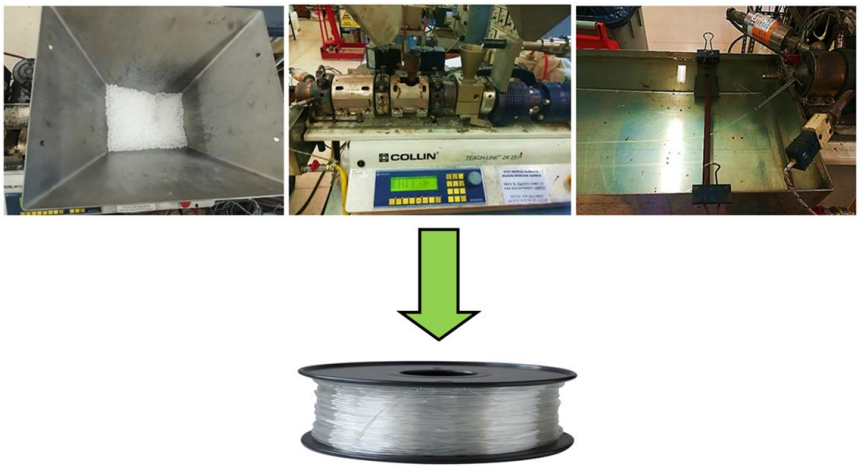

Figure 6: Filament elaboration parts. 1) PET pellets 2) configuration of extruder´s parameters 3) water bath.

III.ili 3D Printing and Printer Parameters

In this study, a TUMAKER Voladora V1 FFF printer was used, figure 7.

Figure 7: TUMAKER Voladora V1 FFF machine. Retrieved from: https://tumaker.com/en/shop/printer/voladora-nx-hd

The printed product is designed and controlled with Simplify3D software by Creative Tools AB. This software generates the requiring G-code and controls the printing parameters. Since the primary purpose of this research is mechanical testing, the printing product is the specimen shown in figure 8, that obeys the ASTM D638 standards[22]. The nozzle diameter is 0.4 mm, and the employed filament has a nominal diameter of 1.70 mm.

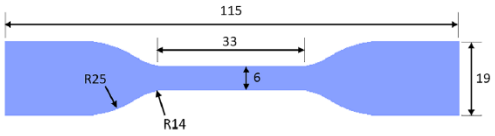

Figure 8: Dimensions of the tensile test specimen following the ASTM D638, type IV standards. The dimensions are expressed in mm, and the specimen's thickness is 3.20mm. Adapted from reference (3).

Furthermore, to establish the most adequate printing conditions, seven different combinations of variables were performed as shown in Table I. For this purpose, the three parameters that were taken into account were printing velocity, bed temperature, and nozzle temperature.[4] The name XZY of the printing conditions refers to the variable that is changed. X stands for nozzle temperature, Y for bed temperature, and Z for printing velocity. However, other important printing parameters, such as layer height and fill density, were kept constant at 0.27 mm and 100%, respectively.

The rectilinear 0º fill pattern was established for printing the tensile-test specimens. However, few attempts were made using the concentrical fill pattern. The tensile test was not carried out for the concentrical printed specimens[23]. The visual differences between the two patterns are shown in figure 9. Further printing conditions are mentioned in the tables of Appendix I.

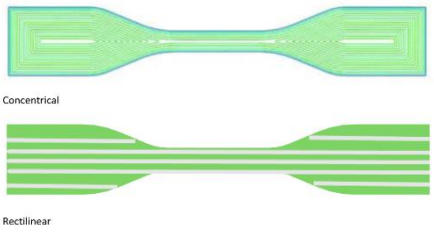

Figure 9: Tensile test specimens printed in two different fill patterns. Above printed specimen in concentrical pattern. Below the specimen with rectilinear fill pattern.

Apart from printing specimens for the tensile test, according to ASTM D638 standards[22], specimens for the welding strength test were also printed. Following the ASTM1938-19[24]

geometry, the seven aforementioned printing conditions were applied. The particularity of this case is that the printing process has to be paused, between the 41st and 42nd printed layer, to place the aluminium paper and then print over it, as it is shown in figure 10. The presence of the aluminium paper is to cause a pre-crack of 60mm.

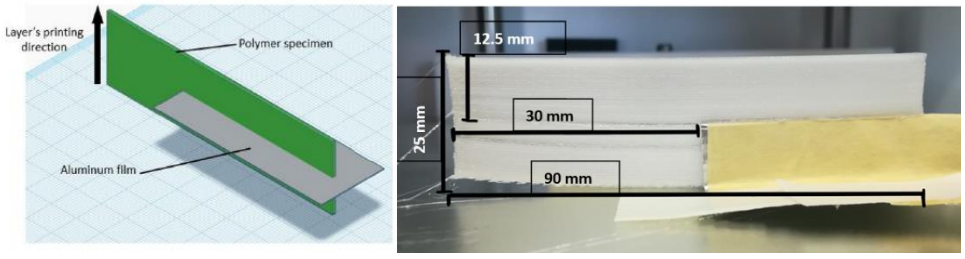

Figure 10: Placement of aluminium paper in the trouser test specimen. Adapted from reference (20).

Table I: Printing conditions for tensile test and trouser test specimens.

# Specimen	**XYZ** CONDITION	Nozzle Temperature (ºC)	Bed Temperature (ºC)	Printing Velocity (mm/s)
1	A1a	270	100	30
2	B1a	275	100	30
3	C1a	280	100	30
6	C2a	280	85	30
7	C3a	280	70	30
5	C1b	280	100	25
4	C1c	280	100	20

III.iv Injection Moulding

The mechanical and thermal properties of the printed specimens are to be compared with specimens that are obtained by the traditional injection process. In this case, it is also crucial to dry properly the PET resin before injection.

Figure 11: Battenfeld BA-230-E injection machine.

The presence of water molecules can affect the mechanical properties due to the formation of bubbles and/or the hydrolysis of the material. The PET pellets were placed for 72h in a dehumidifier at 70 ºC. For the injection process, the Battenfeld BA-230-E injection machine was used, figure 11. This machine contains one reciprocating screw of 18 mm diameter, an L/D ratio of 17.8 and a maximum closing force of 23 tones.[20] As mentioned above, three mould temperatures have been used: 25, 70 and 85 ºC, similar to the bed temperature conditions. The melt temperature will be 270 ºC. In Table II, the three injection conditions are listed.

Table II: Specimen injection conditions.

# CONDITION	Melt Temperature (ºC)	Bed Temperature (ºC)	Extrusion Speed (cm/s)
A1a	270	25	11.43
B1a	270	70	11.43
C1a	270	85	11.43

III.v Differential Scanning Calorimetry DSC

PET is a semi-crystalline polymer. The percent crystallinity is a very important property to be measured. This parameter gives the overall level of the crystalline component. Depending on the percent crystallinity of the thermoplastic material, the mechanical properties like toughness, brittleness and modulus vary. In addition, the optical clarity changes from a more transparent one for the amorphous state, to an opaque one for the more crystalline state[25,26].

The semicrystalline polymers contain a complex structure that is formed by crystalline and amorphous regions. In general terms, the crystalline parts are formed by lamellas of crystallized polymer chains, where the chains are folded and aligned in a crystallographic register within the thin lamellae. The crystalline lamellae are separated by amorphous regions and the lamellae and the interlamellar amorphous regions assemble into spherical superstructural entities called spherulites. On the other hand, the amorphous region lacks orientation and the polymer chains are disordered. In some materials, such as PET, the crystallinity can be induced by heating above the glass transition temperature, T_g. This process is known as cold crystallization. Hence, polymers like PET can exist in the amorphous state when they are quenched rapidly enough below their T_g or they are semi-crystalline when they are slowly cooled from the melting state.[27] Crystallinity depends on many factors like the molecular weight of the polymer, the polymer chain structure, the crystallization temperature.

Particularly, crystallinity in PET can be induced either by heating -*thermal crystallization*- or stress or strain crystallization. In thermal crystallization, superstructures called spherulites are generated and the polymer turns opaque. In stress-strain crystallization, the polymer chains are rearranged and closely packed [28].

In the 3D printing process, the printing velocity and the bed temperature are expected to have a significant influence on the percent of crystallinity, as shown in figure 12. On the other hand, the mould temperature in the injection process can have a huge effect, too.

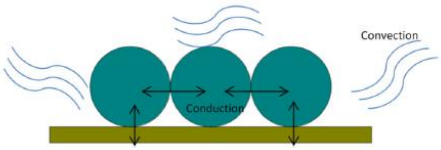

Figure 12: A schematic of heat transfer mechanisms in deposition stage: conduction between rasters and layers and bed, and convection between rasters and ambient. Adapted from reference (27).

In order to obtain the thermal properties and the crystallinity degree, a Perkin Elmer DSC 8000 equipped with an Intracooler 2 has been used. The scans were carried out under a constant ultra-pure nitrogen flow. The samples of about 5 to 7 mg were encapsulated in standard aluminium pans. Since the main objective is to know the thermal properties and the degree of crystallinity of the obtained parts, only a single heating sweep was programmed. The samples were, therefore, heated from 0 ºC to 290 ºC at a heating and cooling rate of 20 ºC/min.

The melting temperature, T_m, and cold crystallization temperature, T_{cc}, were calculated at the maximum and minimum points, respectively, of the DSC scan. The endothermic processes, such as melting, are drawn upwards, figure 13.

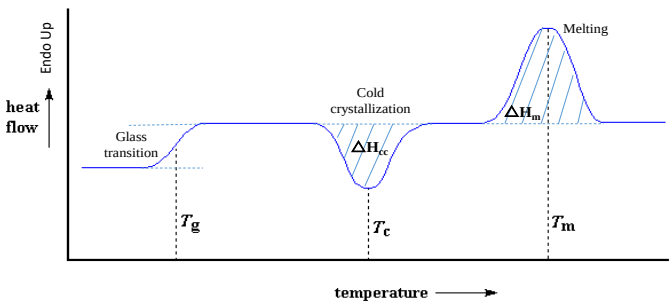

Figure 13: DSC analysis of a semicrystalline polymer. Endothermic processes are drawn upwards while the exothermic ones appear downwards. Adapted from reference(26).

The crystallinity degree was calculated from the fusion enthalpy, in accordance with the following equation:

$$Xc = \frac{\Delta H_m - \Delta H_C}{\Delta H_m^o} * 100 \quad (1).$$

In this equation, ΔH_m is the melting enthalpy and ΔH_C the cold crystallization. They are determined by integrating the obtained peaks in J/g, shown in figure 13. The presence of a cold crystallization peak may not always appear as it depends on the nature of the material. ΔH_m^o is the fusion enthalpy of a 100% crystalline polymer. PET in a 100% crystalline state has a 140.1 J/g fusion enthalpy[25].

III.vi Dynamic Mechanical Thermal Analysis (DMTA)

The thermal properties of polymers are characterized by two important temperatures, the glass transition temperature T_g and the melting temperature T_m. The most suitable technique for T_m characterization is DSC, as described above. However, the characterization of the glass transition state of the semi-crystalline materials is sometimes difficult using this technique, due to the low intensity of the signal. Usually, in semi-crystalline materials, the fraction of amorphous materials responsible for this transition is small and therefore, the signal in DSC is of low intensity. For this reason, the use of other techniques, such as DMTA, is required to characterise this transition more precisely.

Dynamic Mechanical Analysis, otherwise known as DMA, is a technique where a small deformation is applied to a sample in a cyclic manner. The response of the materials to stress, temperature, frequency, and other values can be studied. DMA measures the stiffness and damping which are reported as modulus and tan δ.[29] Since we are applying a sinusoidal force, we can express the storage modulus as an in-phase component and the loss modulus as an out of phase component. The storage modulus, either E' or G', is the measure of the elastic behaviour of the sample. The ratio of the loss modulus to the storage modulus is the tan δ and is often called damping. It is a measure of the energy dissipation of a material [30].

In this work, the DMTA has been used mainly to determine the glass transition temperature of the different specimens. An equipment Triton 2000 DM, from Triton Technology, was used in bending deformation mode with a single cantilever clamp, figure 14.

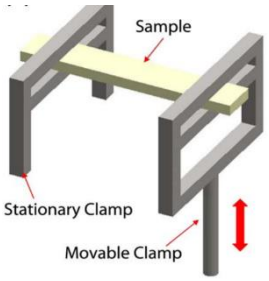

Figure 14: Single cantilever clamp with the sample placed. Adapted from reference (31).

The samples of approximately 10mm long, were heated from 0 ºC to 120 ºC at a constant rate of 4 ºC/min and a constant frequency of 1 Hz. As to obtain a linear viscoelastic response, low strain amplitudes were applied. Lastly, the T_g was determined as the maximum of the tan δ peak.

III.vii Tensile Testing

The most important part of this study is the evaluation of the mechanical properties that the final products made out of PET have. Specimens obtained from two different methods, injection and FDM technology, and under different elaboration conditions are to be tested. According to the ASTM D638 standards[22], tensile stress-strain tests will be performed by a universal testing machine INSTRON 5569 with a test speed of 20 mm/min. The specimens have been obtained on the previous steps, and they have a type IV and are dumbbell-shaped, as shown in figure 15.

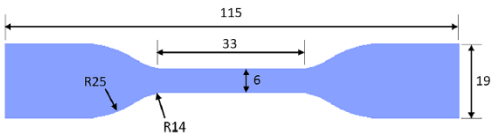

Figure 15: Dimensions of the tensile test specimen following the ASTM D638, type IV standards. The dimensions are expressed in mm and the specimen's thickness is 3.20mm. Adapted from reference (3).

Among the properties that can be obtained are yield strength, tensile strength, Young´s modulus, and elongation at break. The International Organization for Standardization applies the ISO 527 for the tensile characterization of plastics in order to calculate the tensile stress/strain ratio under specific conditions[31].

From the graphs, the Young´s modulus, the deformation percentage and the yield strength will be taken into consideration. For each particular case, at least five specimens have been tested to have the average values of each mechanical property[32,33].

III.viii Welding Strength testing

One of the problems that one can face in FDM printing is the presence of weak weld between subsequent layers of the extruded material. Welding tests have to be run to achieve the highest possible welding strength so as to optimize the processing parameters. The average torsional tearing energy of strip of material is to be determined by a Mode III "trouser tear" fracture experiment[34].

ASTM 1938 covers the standard for the determination of tear propagation resistance of a plastic film. This method is not adequate for brittle plastics. Since the adhesion between the layers has to be determined and there is no official standard method to measure it, ASTM 1938-19 standard will be applied [24]. The geometry of the specimens and tear testing parameters obey the ASTM D1938-14 standards. The tested specimen is printed as shown in figure 16, and a pre-crack of 60 mm is built to determine the interfacial bonding.

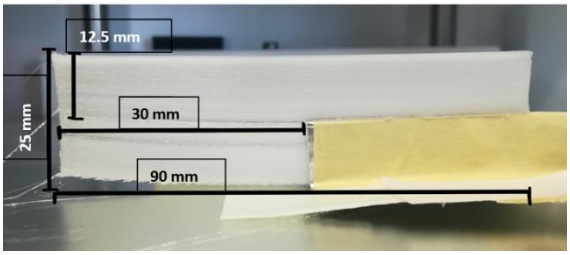

Figure 16: Dimensions of trouser specimen. The thickness of the specimen is 1mm.

Once the small slit is introduced, in one of the short ends and then the two tabs are manually separated, figure 17.

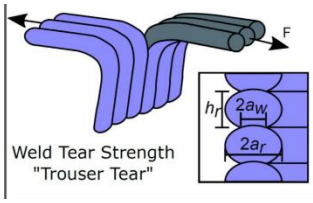

Figure 17: Trouser-test specimen tear direction. Adapted from reference (34).

The experiment has been carried out by a universal INSTRON 5569 testing machine with 50mm of the distance between the jaws and a test speed of 254 mm/min.

III.ix Scanning Electronic Microscope SEM

The cross-sectional morphology of the printed specimens has been analysed by Scanning Electron Microscope (SEM). The difference between the two filling patterns will be compared, and most importantly, the influence of the processing parameters of FDM technology on the internal morphology of the specimens will be observed. To obtain the observation surfaces, the samples were placed in liquid nitrogen for 1 hour to produce a cryogenic fracture. The SEM observation has been performed with Hitachi TM3030 Plus microscope with accelerating voltages of 15 kV. Previously, the tested samples had to get their surface coated with gold by Bio-Rad Microscience Division SC500 sputter Coater, figure 18 [35].

Figure 18: Bio-Rad Microscience Division SC500 sputter Coater.

IV. RESULTS AND DISCUSSION

Since one of the aims of this study is to achieve good mechanical properties by printing specimens, the mechanical properties of the injected specimens will be evaluated first. The mechanical and thermal behaviour of the specimens obtained by injection moulding will be analysed.

*IV.i **Injected Specimens***

Figure 19 shows the specimens obtained by injection moulding according to the injection conditions of Table II. As can be seen, there are clear differences in the transparency/opacity of the samples resulting from the different temperatures of the mould. When the temperature of the mould rises (85 ºC), the specimen is no longer transparent since it crystallizes.

Figure 19: Injected specimens at three different mould temperatures. From left to right the mould temperature increases. (25, 70 and 85 ºC).

IV.i.a Tensile Test

Table III and Figure 20 to 22 show the results obtained for the tensile tests of the injected samples at different mould temperatures. (Young´s modulus, deformation at break and yield strength)

Table III: Young´s modulus for ASTMD38 injected specimens at different mould temperatures.

# CONDITION	Mould Temperature (ºc)	Young´s Modulus (Mpa)	Elongation at break (ε_b,%)	Yield Stress (MPa)
A1a	25	2670 ± 42	286 ± 10	59 ± 1
B1a	70	2600 ± 30	260 ±27	59 ± 1
C1a	85	2420 ± 123	260 ±52	56 ± 4

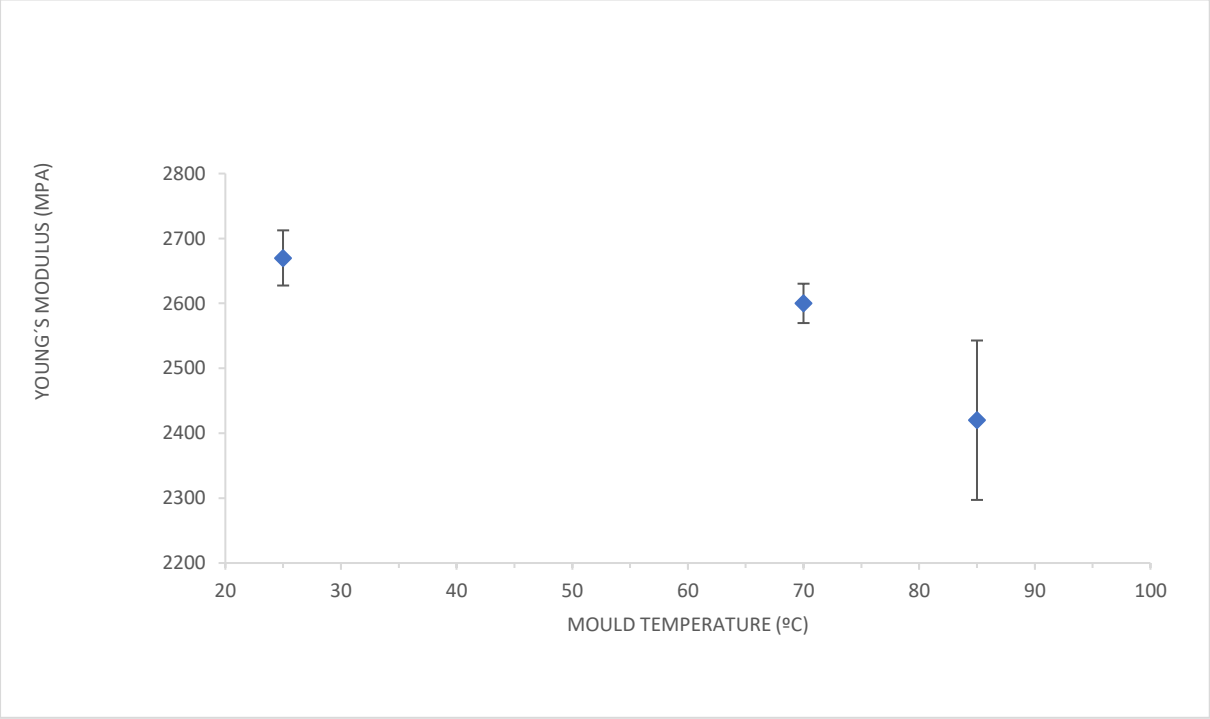

Figure 20: Young´s Modulus of injected specimens in the function of the mould temperature obtained in the tensile test.

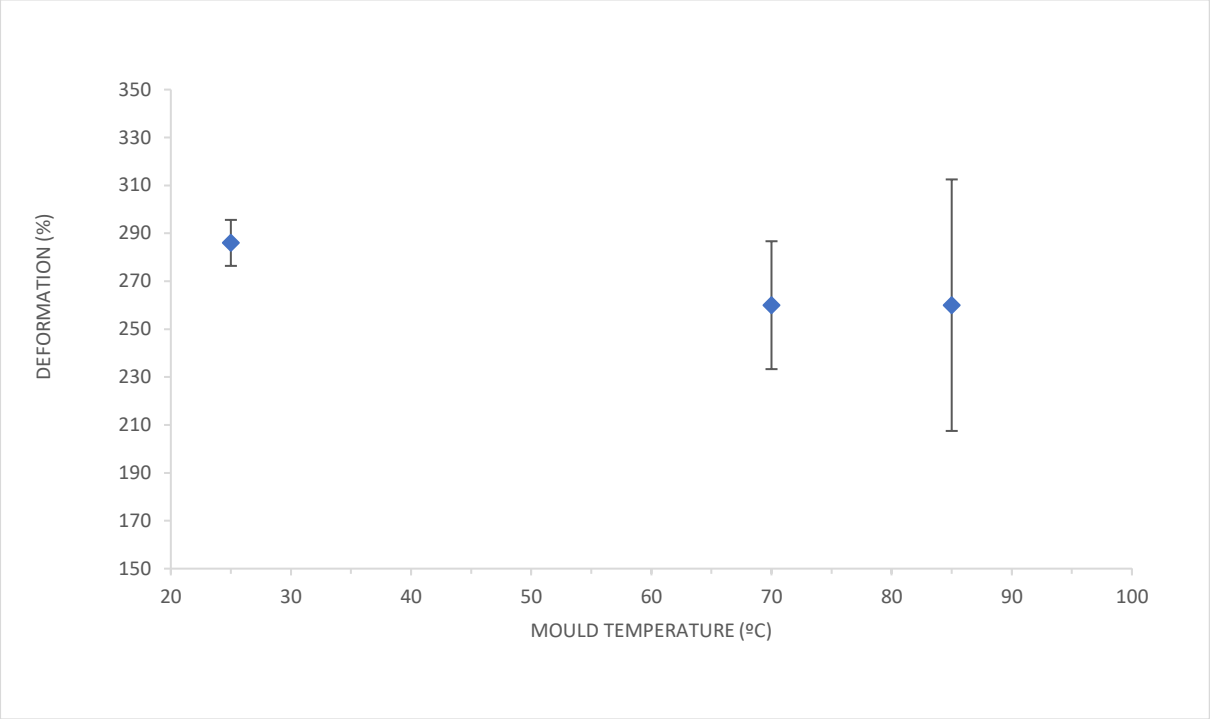

Figure 21: Elongation at break of injected specimens in the function of the mould temperature obtained in the tensile test.

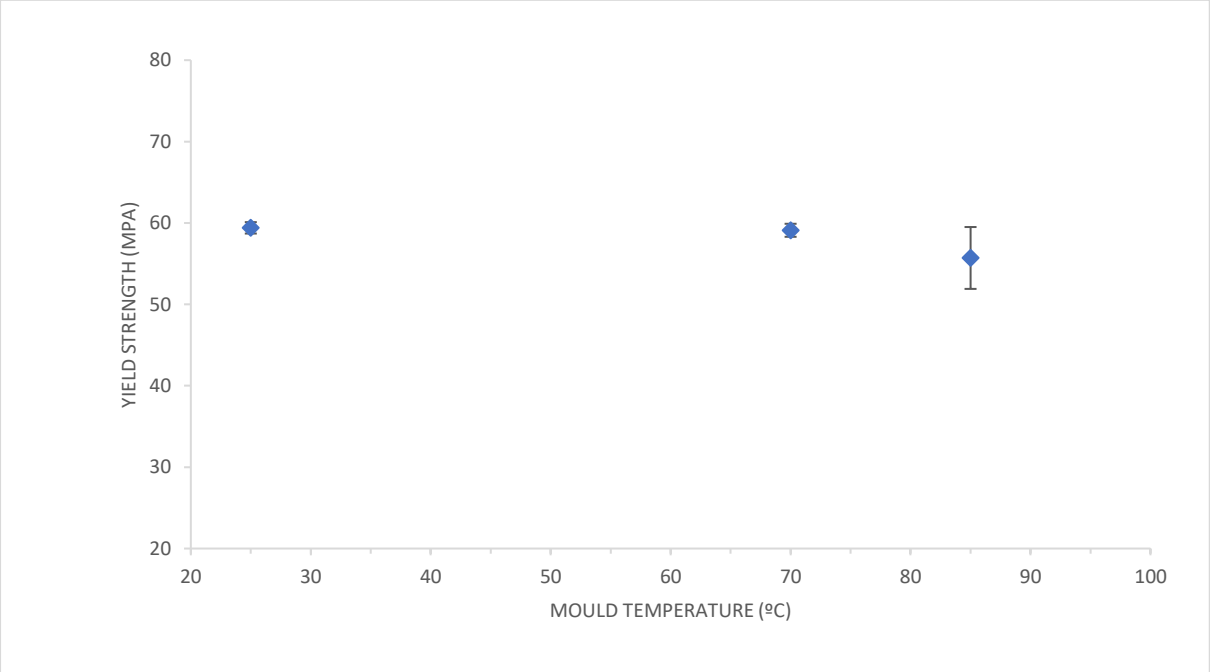

Figure 22: Yield strength of injected specimens in function of the mould temperature obtained in the tensile test.

As can be seen, the increase of the mould temperature results in a slight decrease in Young´s Modulus and a slight decrease of the deformation at break but has no significant influence on yield strength. Nevertheless, a higher modulus was expected accompanied by a reduction in the elongation at break. Those results are in agreement with those obtained for virgin PET, being related to the crystallinity degree of the test bars.[36,37]

IV.i.b Differential Scanning Calorimetry

Figure 23 shows the first DSC heating scans of the samples injected at different mould temperatures. It should be noted that DSC first heating scans reflect the thermal history of the samples. Table IV contains the values of cold crystallization temperatures, T_{cc}, melting temperatures, T_m, and crystallization degree (X(%)).

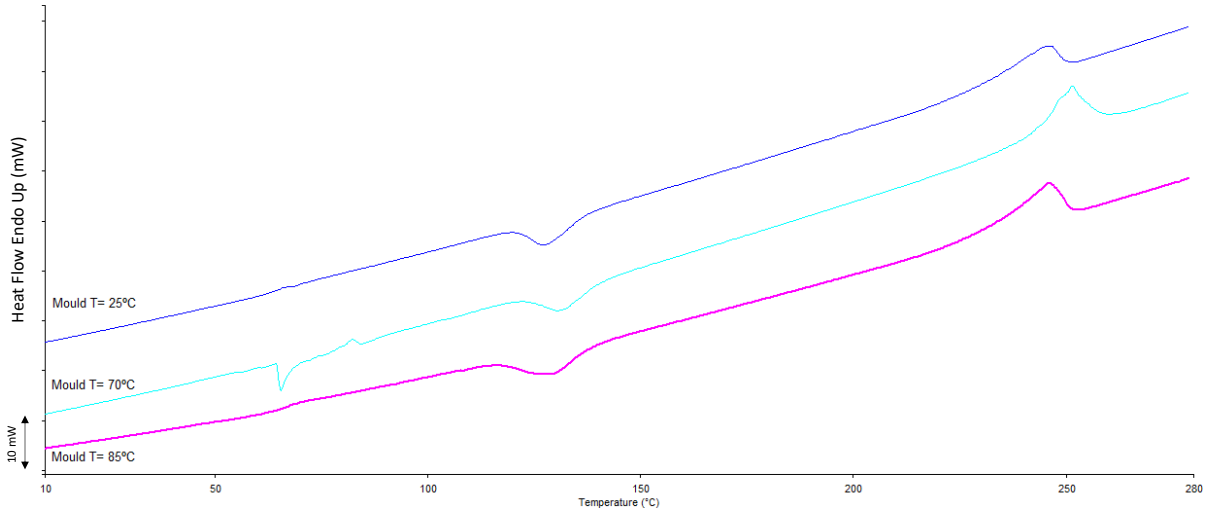

Figure 23: DSC first scan for the injected specimens at three mould temperatures. Blue curve T=25 ºC. Light blue line T= 70ºC. Pink line T= 85 ºC.

Table IV: Thermal properties of injecting moulded specimens.

# CONDITION	Mould Temperature (ºC)	T_{cc} (ºC)	T_m (ºC)	Crystallinity (%)
A1a	25	129	256	2
B1a	70	131	251	11
C1a	85	127	245	2

DSC results show the presence of a cold crystallisation exotherm, once T_g is exceeded, followed by a melting endotherm. T_{cc} changes along with the mould temperature but with an undefined pattern. From A1a condition to the B1a condition where the mould temperature rises the T_{cc} rises too. However, when the mould temperature increases from B1a condition to C1a, the T_{cc} decreases. There is no explanation for this phenomenon. On the other hand, a reduction in the T_m value can be observed when the mould temperature rises. In addition, the degree of crystallinity is affected by the mould temperature as well. As shown, when the mould temperature rises from 25 ºC to 70 ºC, an increase of crystallinity degree is observed. This is an expected result, as 70ºC corresponds to a temperature very close to the beginning of the glass transition, so there is some mobility of the polymer chains to fold back into crystalline regions. Nevertheless, the crystallinity degree obtained for the sample moulded at T = 85ºC (C1a) is the same as the sample moulded at T=25ºC. This result would indicate that the sample moulded at 85ºC has a higher amorphous fraction than the one moulded at 75ºC, which is not logical since at 85ºC the segmental and chain mobility is even higher. In addition, it is important to mention that the test specimen obtained at 85ºC shows a pale white colour, which became more pronounced on going from the surface to the centre. This could indicate that there is a crystallinity gradient between the surface and the centre of the specimen. The same observation was already made by Müller et al. in their study focusing on the thermal and mechanical properties of PET from beverage bottles. In this study, the authors noted differences in the degree of crystallinity of samples taken from the surface and core of PET specimens injected at temperatures even lower than the T_g of the PET. [38]Therefore, this result

would be understandable considering that the sample taken for the DSC scan is from the surface of the specimen.

IV.ii ***Printed Specimens-RECTILINEAR fill pattern***

As mentioned in the experimental section, several printing parameters have been evaluated, as shown both in Table I and below, in which the name XZY of the printing conditions refers to the variable that is changed. X stands for nozzle temperature, Y for bed temperature and Z for printing velocity.

Table I: Printing conditions for tensile test and trouser test specimens.

# Specimen	**XYZ** CONDITION	Nozzle Temperature (ºC)	Bed Temperature (ºC)	Printing Velocity (mm/s)
1	A1a	270	100	30
2	B1a	275	100	30
3	C1a	280	100	30
6	C2a	280	85	30
7	C3a	280	70	30
5	C1b	280	100	25
4	C1c	280	100	20

As far as the raster orientation is concerned, mainly a 0º raster orientation has been used. That means that the specimen has been produced by arranging the filaments in parallel in order to achieve better mechanical properties. Only for comparative purposes, some printing

attempts have been made with a concentric raster. In Figure 24 the printed tensile-test specimens are shown:

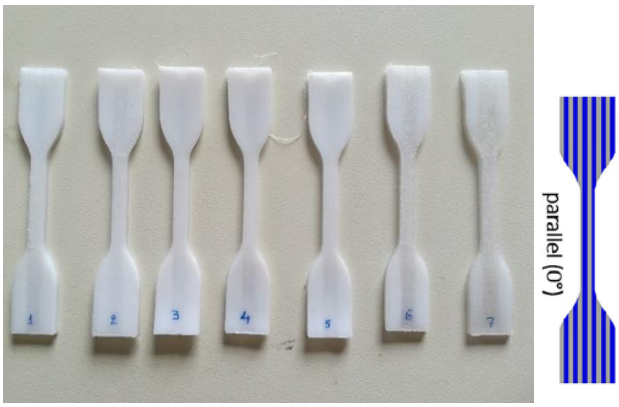

Figure 24: Tensile-test specimens printed at seven different conditions with a rectilinear fill pattern.

The mechanical properties obtained for the different printing conditions are shown as follows. What is important to note at this point, is that in none of the cases were yield stress results obtained due to the fragility of the samples, i.e., they did not undergo yielding during the test.

IV.ii.a. Tensile Test

IV.ii.a.1 The nozzle temperature effect

The nozzle temperature effect is firstly observed for (1,2,3) specimens printed by A1a, B1a and C1a conditions as shown in Table V and figure 25-26.

Table V: Nozzle Temperature effect on the mechanical properties.

# Specimen	XYZ CONDITION	Bed Temperature (ºC)	Printing Velocity (mm/s)	**Nozzle Temperature (ºc)**	**Young´s Modulus**	**Elongation at break (%)**
1	A1a	100	30	**270**	**2292 ± 66**	**2 ± 0.4**
2	B1a	100	30	**275**	**2305 ± 77**	**3 ± 0.5**
3	C1a	100	30	**280**	**2390 ± 95**	**3 ± 0.7**

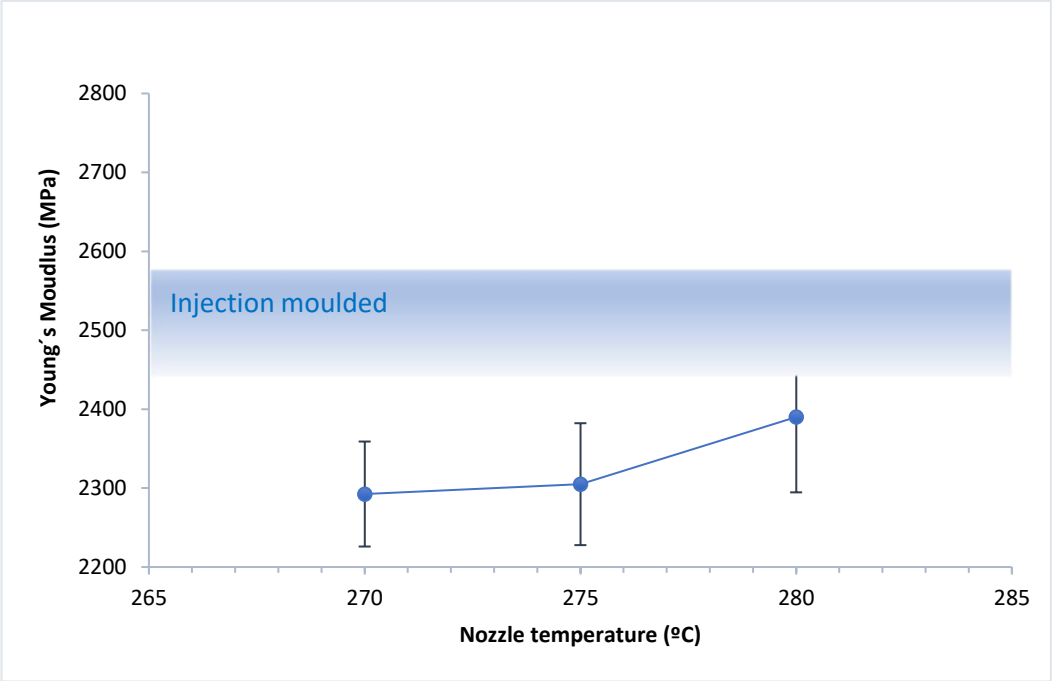

Figure 25: Representation of Young´s Modulus values with the error bars, obtained by the printed specimens at different nozzle temperatures. The shaded area corresponds to Young's modulus values obtained for the injected specimens.

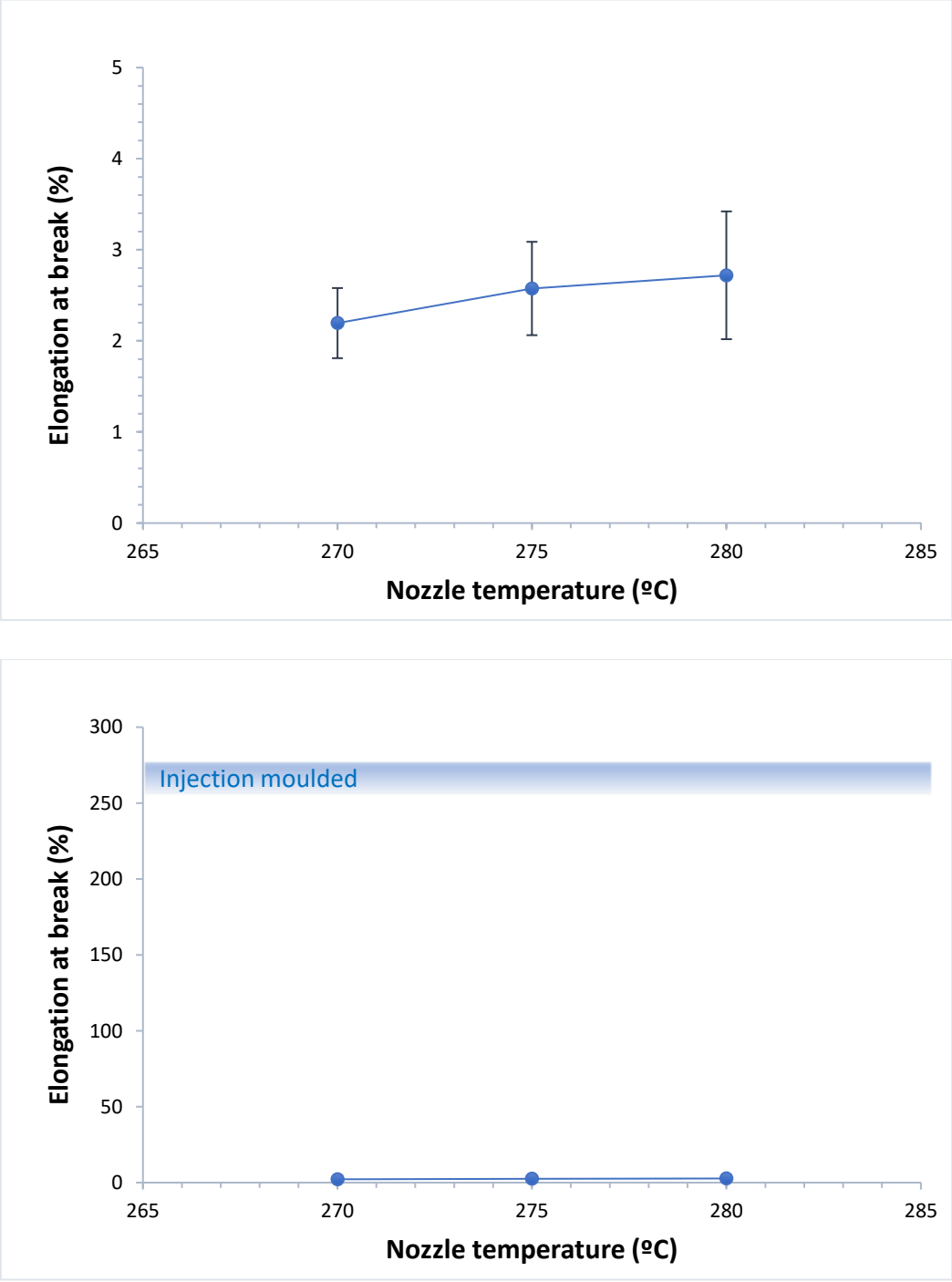

Figure 26: Representation of the deformations % values with the error bars, obtained by the printed specimens at different nozzle temperatures. The shaded area corresponds to Young's modulus values obtained for the injected specimens.

These results reveal that an increase of the nozzle temperature causes a slight increase of Young´s modulus and consequently an increase in the stiffness of the material. A higher

percent of crystallinity is to be expected. Nevertheless, these results are lower than those obtained for injected specimens. As far as the elongation at break is concerned, the nozzle temperature seems to have no significant influence on the deformation of the studied material. Similar results were found by Bakir et al. in their work on the effect of FDM process parameters on the mechanical properties of recycled PET parts. [13]They found an increase of about 100% in the strength of the specimens when the nozzle temperature increased from 230ºC to 260ºC; however, this increase had no significant effect on elongation. The monotonic increase in strength with increasing nozzle temperature was associated with the improvement in the fusion quality between printed lines. For most specimen geometries, the time between the printing of adjacent lines is long enough to result in the complete solidification of the first polymer line. Therefore, the integrity of the specimen relies on the heating induced by the incoming line, which partially melts the existing printed lines. As the temperature of the incoming polymer line increases, the heat-affected zone widens, the fusion improves, and the morphological irregularities causing stress concentrations to disappear. After comparing the elongation values obtained for the injected specimens to the printed ones, the elongation values of the 3D specimens are significantly lower. This observation is probably related to the degree of crystallinity achieved, as the specimens produced by 3D look opaque and not transparent like the injected ones.

IV.ii.a.2 The bed temperature effect

Secondly, the bed temperature effect is observed for (3,6,7) specimens printed by C1a, C2a and C3a conditions as shown in Table VI and figure 27-28.

Table VI: Bed Temperature effect on the mechanical properties.

# Specimen	# CONDITION	Nozzle Temperature (ºC)	Printing Velocity (mm/s)	**Bed Temperature (ºC)**	**Young´s Modulus (MPa)**	**Elongation at break (%)**
7	C1a	280	30	**70**	**2035 ±70**	**3 ± 0.7**
6	C2a	280	30	**85**	**2005 ±75**	**3 ± 0.7**
3	C3a	280	30	**100**	**2390 ±95**	**3 ± 0.9**

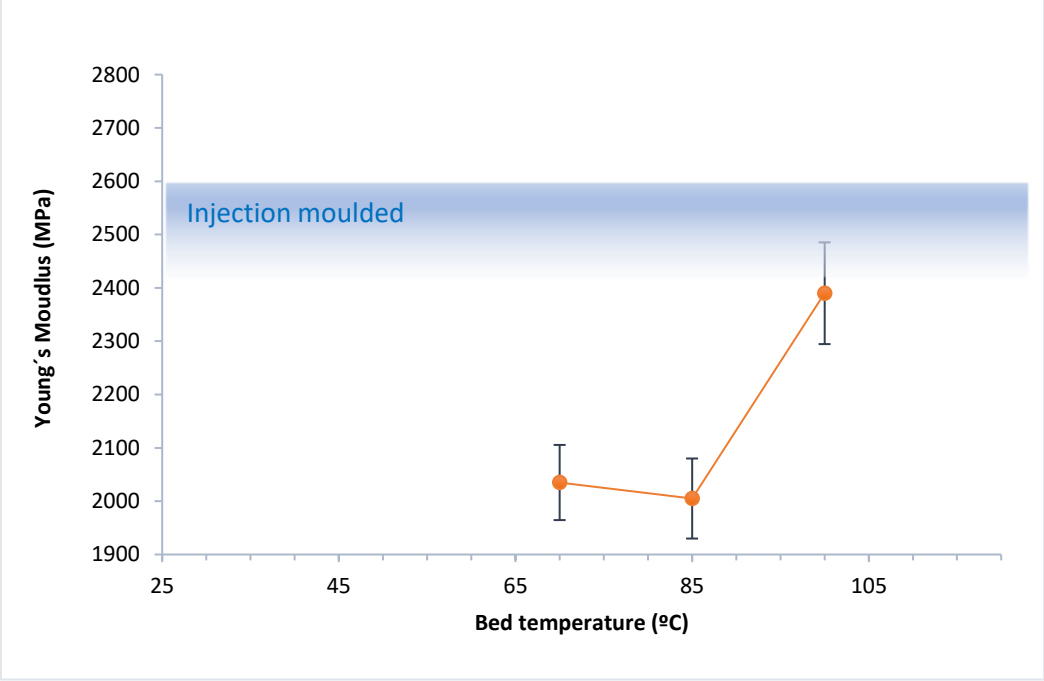

Figure 27: Representation of Young´s Modulus values with the error bars, obtained by the printed specimens at different bed temperatures. The shaded area corresponds to Young's modulus values obtained for the injected specimens.

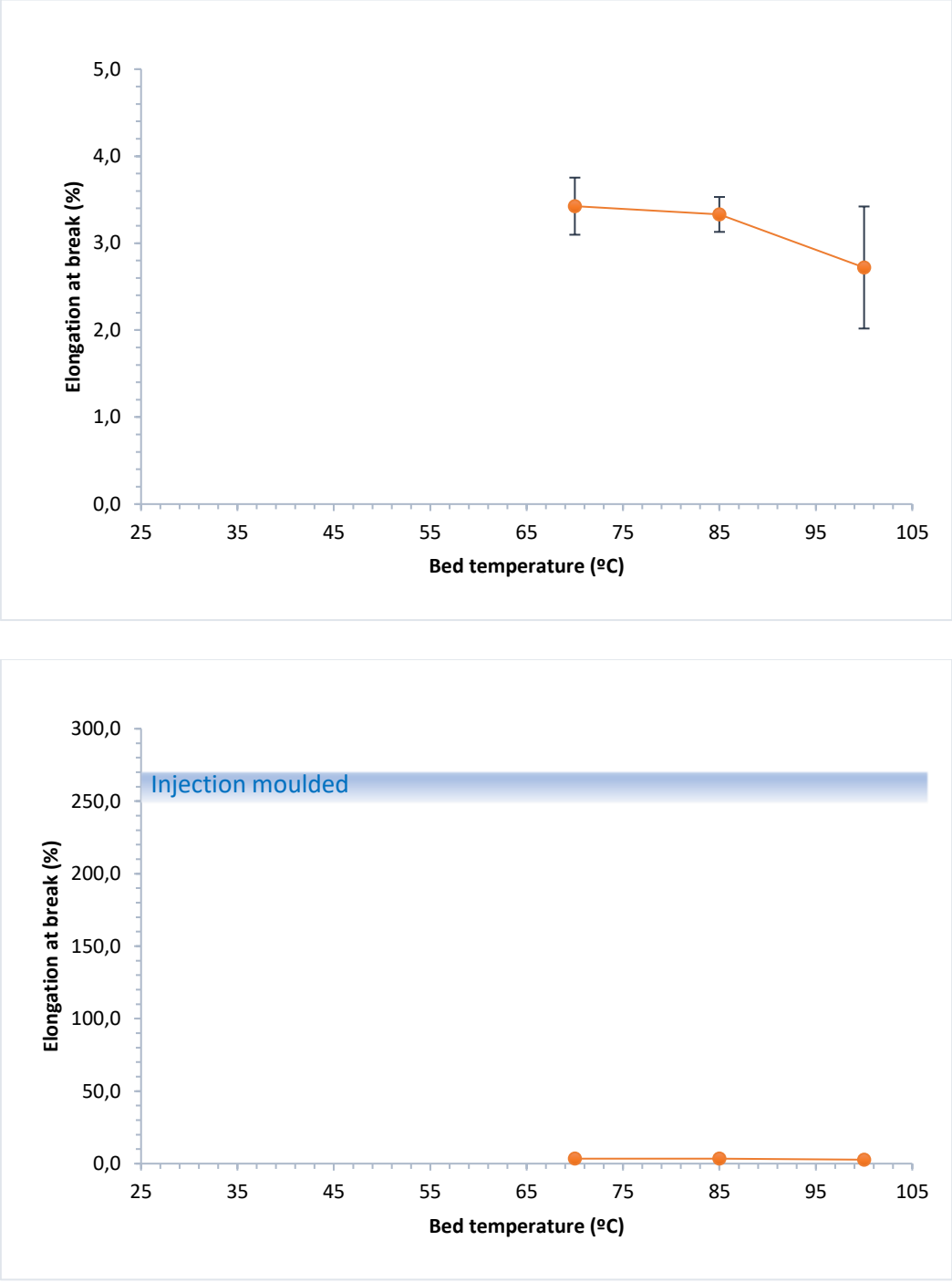

Figure 28: Representation of the deformations % values with the error bars, obtained by the printed specimens at different bed temperatures. The shaded area corresponds to Young's modulus values obtained for the injected specimens.

The increase of the bed temperature from 70 ºC to 100 ºC leads to an important increase in Young´s modulus, decreasing the gap with the injection moulded specimens. It is not possible

to directly compare the literature results to our findings. Nevertheless, the results suggest that the rise in the bed temperatures favours the crystallization of the material and, therefore, the increase of Young's modulus.

As far as the elongation at break is concerned, the nozzle temperature seems to have little influence on the deformation of the studied material. As observed from the graphical representation above, the increase in the bed temperature seems to decrease the elongation at break. However, it is not significant compared to the values obtained for the injected moulded specimens.

IV.ii.a.1 The printing velocity effect

The printing velocity effect is observed for (3,4,5) specimens printed by C1a, C1b and C1c conditions as shown in Table VII and figure 29-30.

Table VII: Printing Velocity effect on the mechanical properties.

# Specimen	# CONDITION	Nozzle Temperature (ºC)	Bed Temperature (ºC)	**Printing Velocity (mm/s)**	**Young´s Modulus (MPa)**	**Elongation at break (%)**
3	C1a	280	100	**30**	**2228 ±54**	**3 ±0.7**
5	C1b	280	100	**25**	**2325 ±99**	**2 ±0.6**
4	C1c	280	100	**20**	**2390 ±95**	**2 ±0.3**

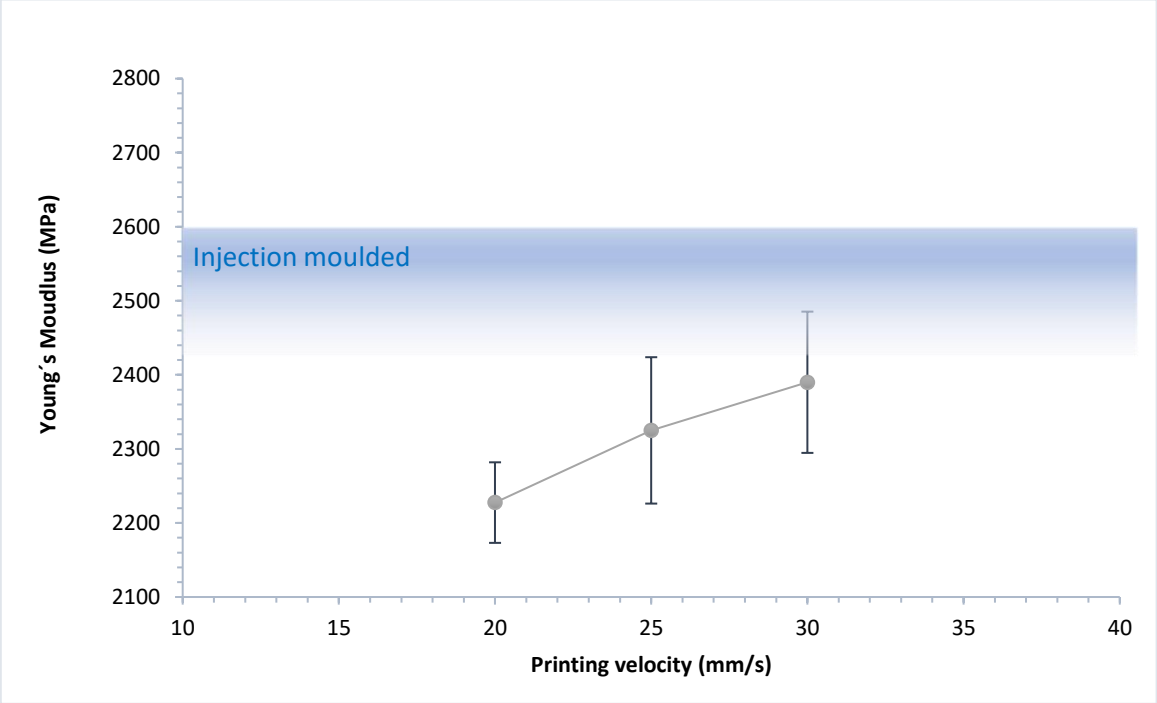

Figure 29: Representation of Young´s Modulus values with the error bars, obtained by the printed specimens at different printing velocities. The shaded area corresponds to Young's modulus values obtained for the injected specimens.

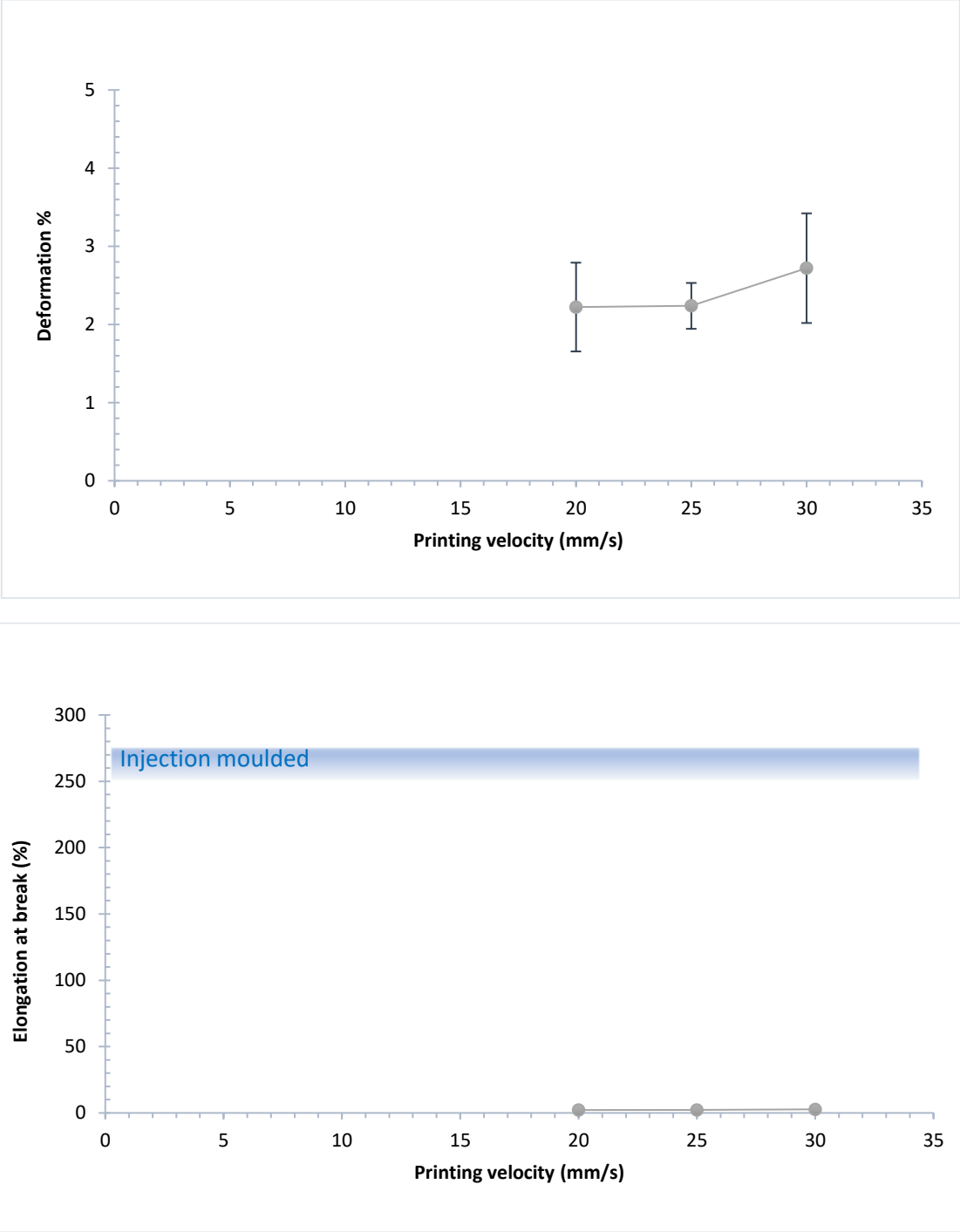

Figure 30: Representation of the elongation at break (%) values with the error bars, obtained by the printed specimens at different printing velocities. The shaded area corresponds to Young's modulus values obtained for the injected specimens.

There appears to be little influence of the printing velocity on Young's modulus. However, there is just a small increase in the Young´s modulus as the printing rate increases. The error gap is quite wide so that no meaningful conclusions can be drawn. If this trend is true, though,

an increase in printing speed may lead to some increase in filament crystallinity, as PET is susceptible to crystallisation during stretching.[39] It is crucial to analyse the thermal properties of these specimens to confirm this assumption. As far as the deformation at break is concerned, there is hardly any clear effect on this parameter with printing velocity. The values of deformation at break continue to be much lower than those in the injected specimens[40].

IV.ii.b Differential Scanning Calorimetry

The thermal properties of the samples obtained under different printing parameters have been characterised by DSC. This characterisation is expected to explain the resulted mechanical properties.

Most of the printed specimens visually present an opacity gradient, between the section in direct contact with the bed and the upper surface of the specimen, as shown in Figure 31.

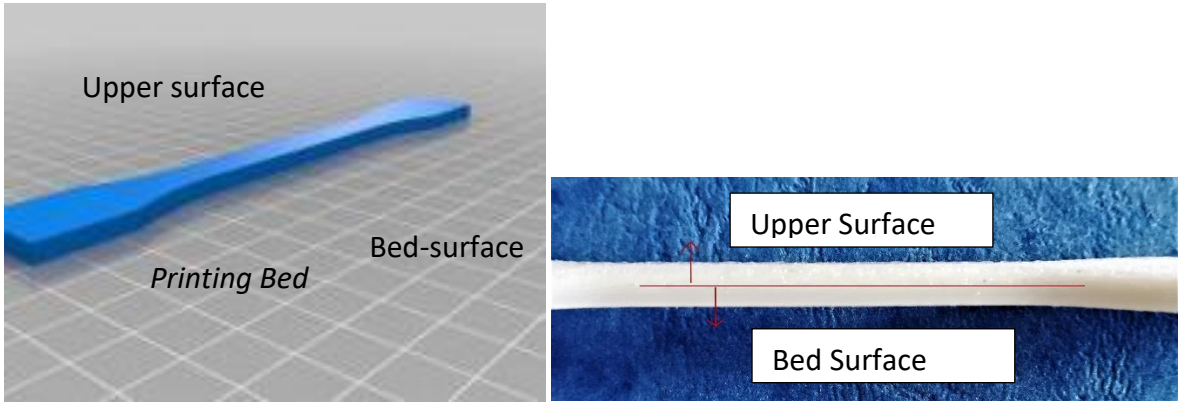

Figure 31: Specimen orientation on the printer bed.

This opacity gradient is more significant for the lower bed temperature. Consequently, the effect of the bed temperature on the thermal properties will be the first to be evaluated.

Bed temperature effect

In Figure 32 DSC scans of the bed- surfaces for the specimen/conditions 3 and 7 are represented. These specimens have been printed at bed temperatures of 100 and 70ºC respectively. Table VIII contains the main thermal properties obtained from DSC scans.

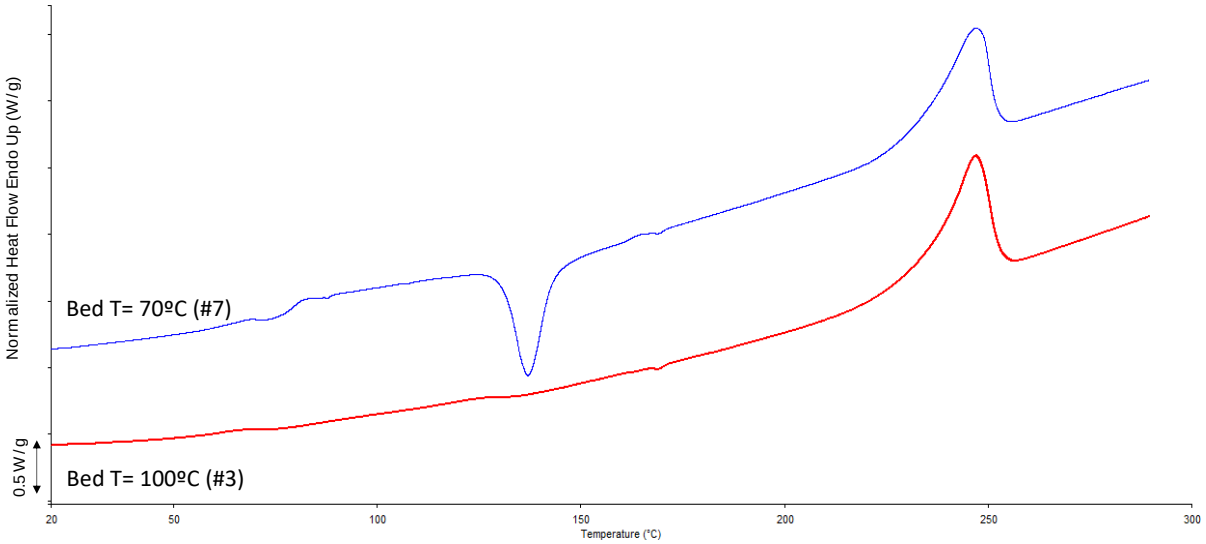

Figure 32: DSC first scan for printed specimens at two different bed temperatures. Red line #3 specimen T=100ºC. Blue line #7 specimen T=70 ºC.

Table VIII: Thermal properties for the printed specimens where the bed temperature is the variable condition.

# Specimen	# CONDITION	Nozzle Temperature (ºC)	Printing Velocity (mm/s)	**Bed Temperature (ºC)**	**Bed Surface Crystallinity (%)**	**Upper Surface Crystallinity %**
3	C1a	280	30	**100**	**27**	**14**
6	C2a	280	30	**85**	**9**	**9**
7	C3a	280	30	**70**	**6**	**7**

As can be seen, the temperature of the bed has a great influence on the degree of crystallinity of PET. However, the melting temperatures are practically the same. Sample/condition 3 (Bed T= 100ºC) shows a higher crystallinity on the surface in contact with the bed than sample/condition 7, obtained at a bed T of 70ºC. This difference could justify the slight improvement in Young's modulus observed in this sample, as well as the small decrease in the elongation at break.

Thus, this difference is clearly seen in the heating sweeps shown in Figure 32. The heating scan corresponding to sample/condition 7 shows a clear cold crystallisation exotherm once T_g is exceeded. This observation indicates that there is a high fraction of crystallisable material whose process has been interrupted by the quenching suffered when deposited on a surface at a temperature slightly below its T_g. However, the sample/condition 3 shows only a small and wide cold crystallisation exotherm, difficult to measure, indicating that most of the crystallisable material has crystallised during processing.

Nozzle temperature effect

In Figure 33 DSC scans of the upper surfaces for the specimen/conditions, 3 and 1 are represented. These specimens have been printed at nozzle temperatures of 280ºC and 270ºC respectively. Table IX contains the main thermal properties obtained from DSC scans.

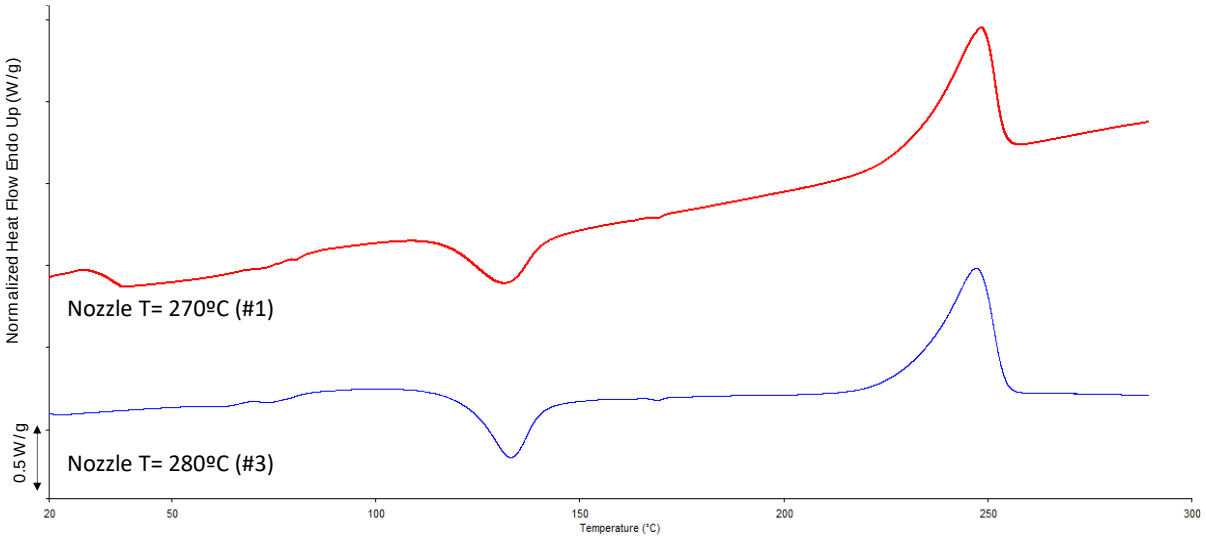

Figure 33: DSC first scan for printed specimens at two different bed temperatures. Red line #1 specimen T=270ºC. Blue line #3 specimen T=280 ºC.

Table IX: Thermal properties measurements for the printed specimens where the nozzle temperature is the variable condition.

# Specimen	# CONDITION	Printing Velocity (mm/s)	Bed Temperature (ºC)	**Nozzle Temperature (ºC)**	**Bed Surface Crystallinity (%)**	**T_{cc} (ºC)**	**T_m (ºC)**	**Upper Surface Crystallinity %**
3	C1a	30	100	**280**	**27**	**133**	**247**	**14**
2	B1a	30	100	**275**	**23**	**134**	**246**	**7**
1	A1a	30	100	**270**	**25**	**132**	**248**	**11**

The cold crystallisation and melting temperatures are similar in all cases. Nonetheless, some improvement in crystallinity is noticed when printing is done at a nozzle temperature of 280ºC. This observation could justify the slight improvement in Young's modulus observed for the sample printed under these conditions. However, a significant crystallinity gap still appears between the surface in contact with the bed and the upper surface. This difference though decreases slightly as the nozzle temperature rises. This could be due to the fact that an increase in the nozzle temperature causes higher overall heating of the layers adjacent to the printing layer, producing a slight crystallinity increase.

Both DSC scans present cold crystallization exotherms, indicating the partially amorphous nature of the upper surface of the specimens.

Printing velocity effect

In Figure 32 DSC scans of the upper surfaces for the specimen/conditions, 3 and 4 are represented. These specimens have been printed at printing velocities of 30 mm/s and 20 mm/s, respectively. Table X contains the main thermal properties obtained from DSC scans.

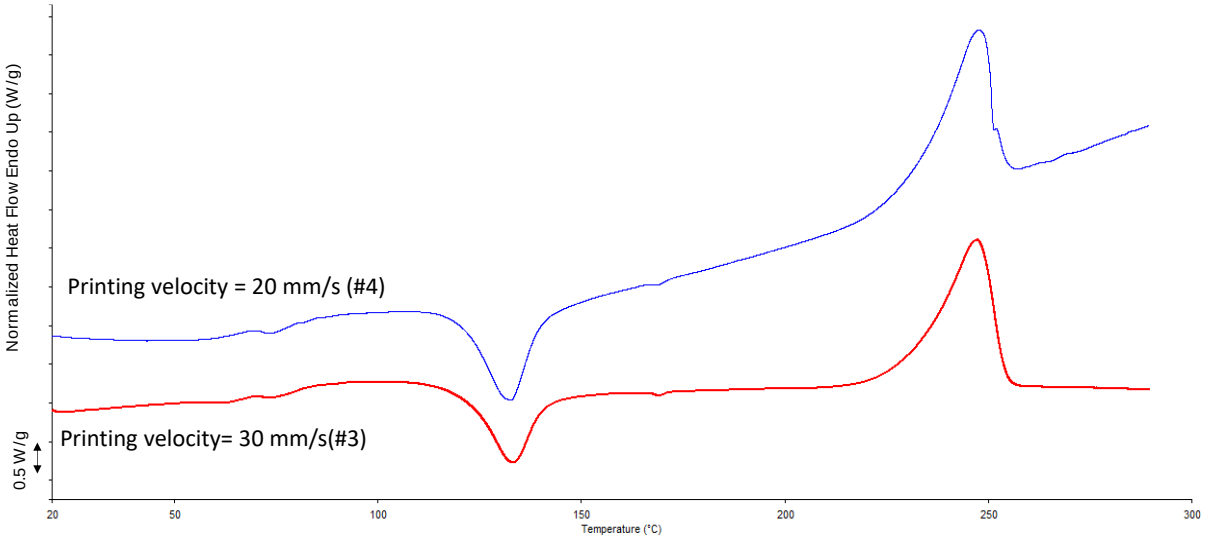

Figure 34: DSC first scan for printed specimens at two different bed temperatures. Redline #3 specimen V=30 mm/s. Blueline #4 specimen V=20 mm/s.

Table X: Crystallinity measurements for the printed specimens where the printing velocity is the variable condition.

# Specimen	# CONDITION	Nozzle Temperature (ºC)	Bed Temperature (ºC)	**Printing Velocity (mm/s)**	**Bed Surface Crystallinity (%)**	**Upper Surface Crystallinity (%)**
3	C1a	280	100	**30**	**27**	**14**
5	C1b	280	100	**25**	**25**	**16**
4	C1c	280	100	**20**	**24**	**7**

As in the previous cases, the cold crystallisation and melting temperatures are very similar. Again, there is a slight increase in crystallinity as the printing velocity increases, which could justify the slight improvement on Young's modulus. The effect of the printing velocity can be somewhat controversial since, on the one hand, a lower printing speed could imply longer times at which the material is subjected to high temperatures, higher than T_g, which could increase the crystallinity. However, higher printing velocities could be crucial for materials such as PET that can crystallise during stretching. In view of the results, it could be thought that the latter effect has more relevance, and the stretching that the material undergoes

during the higher printing velocities favours crystallinity, improving Young's modulus and impairing elongation at break.

The DSC scans depicted in Figure 34 show in both cases cold crystallisation exotherms after T_g. Even though the cold crystallisation exotherm corresponding to sample/condition 3 is relatively smaller, in both cases, the material in the upper layers has a higher amorphous fraction than that deposited directly on the bed.

In this light, it appears that the optimum printing conditions are those corresponding to sample/condition 3, which uses a high nozzle temperature (T= 280ºC), a higher printing velocity (30 mm/s) and a higher bed temperature (T= 100ºC, $T>T_g$). These conditions benefit the crystallisation of the material, slightly increasing Young's modulus. Yet, there is a gradient of crystallinity across the thickness of the specimen that can lead to erroneous conclusions if the results are not treated with some care.

On the other hand, it is important to bear in mind that this crystallinity disfavours the elongation at break, which is much lower than the one obtained in the injected specimens. Nevertheless, some attempts have been made to print PET specimens by keeping the bed at room temperature, in order to produce an amorphous PET specimen, similar to injection moulded specimens. However, no good results have been reached, since the Young's modulus and elongation at break have been 1700 ± 248 and 2 ± 0.1, respectively. These results indicate that must be other factors (structural, adhesion…) behind the poorer mechanical properties of the 3D printed samples.

IV.ii.e Dynamic Mechanical Thermal Analysis (DMTA)

The DSC analysis has revealed the presence of a crystallinity gradient across the thickness of the specimens during the 3D printing. Because of that, it is difficult to give a global crystallinity value for the tensile section, which can later be related to the results obtained.

In addition, the values of the glass transition and the modulus in bending mode will be obtained. The intensity of the signal corresponding to the tan δ is related to the amorphous fraction of the material. However, it contains significant error since PET can have a mobile amorphous phase, a rigid amorphous phase and a crystalline phase. The most appropriate way in determining the crystallinity degree is by DSC or by wide-angle X-ray scattering (WAXS). Thus, relatively high values of tan δ will mean the existence of a larger amorphous fraction, while relatively low values of tan δ will imply a lower content of amorphous fraction. These results will also help to understand the ones obtained for the mechanical properties.

In all the cases, the specimen taken for the test corresponds to the central and narrowest section of the tensile test bar.

Bed temperature effect

Figure 35 shows the DMTA results obtained for the three specimens/conditions in which the control parameter is the bed temperature. Table XI contains the corresponding T_g values and the value of the maximum of tan δ.

Table XI: Glass transition temperature obtained values for rectilinear printed specimens with the bed temperature being the parameter that is changing.

#SPECIMEN	XYZ CONDITION	**Bed Temperature (ºC)**	**tanδ $_{max}$**	**T_g (ºC)**
7	C3a	**70**	1.36	**84**
6	C2a	**85**	1.43	**84**
3	C1a	**100**	0.3	**94**

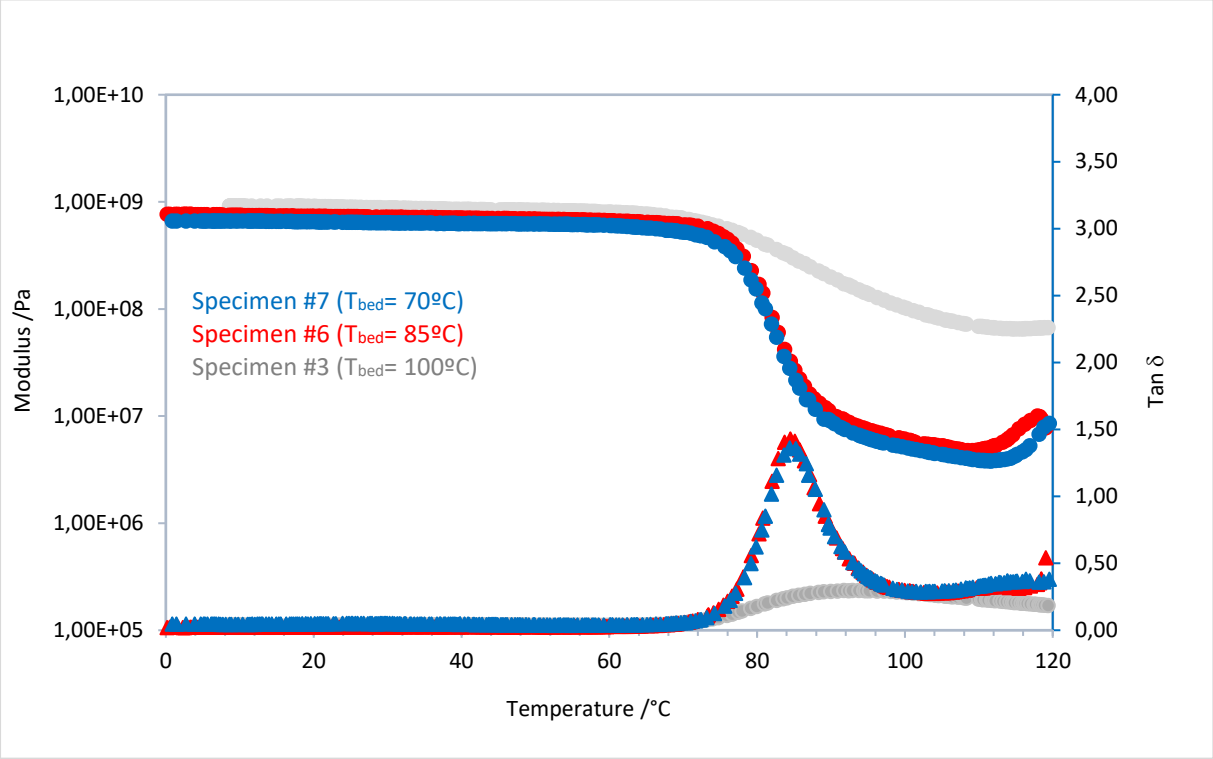

Figure 35: Dynamic mechanical thermal analysis obtained for the printed specimen at three different bed temperatures.

These results show a clear difference between specimens obtained at 100ºC (specimen/condition 3), and specimens obtained at lower bed temperatures. Thus, specimen 3, obtained at a bed temperature of 100ºC presents a maximum tan delta pretty lower than the specimens obtained at bed temperatures of 70 and 85ºC, indicating the presence of a lower amorphous fraction. Furthermore, it presents an elevated T_g value proportional to a higher crystallinity. Those results corroborate the assumptions made so far.

Nozzle temperature effect.

Figure 36 shows the DMTA results obtained for the three specimens/conditions in which the control parameter is the nozzle temperature. Table XII contains the corresponding T_g values and the value of the maximum of tan δ.

Table XII: Glass transition temperature obtained values for rectilinear printed specimens with the nozzle temperature being the parameter that is changing.

#SPECIMEN	XYZ CONDITION	**Nozzle Temperature (ºc)**	**$tan\delta_{max}$**	**T_g (ºC)**
1	A1a	**270**	0.35	**90**
2	B1a	**275**	0.36	**89**
3	C1a	**280**	0.30	**94**

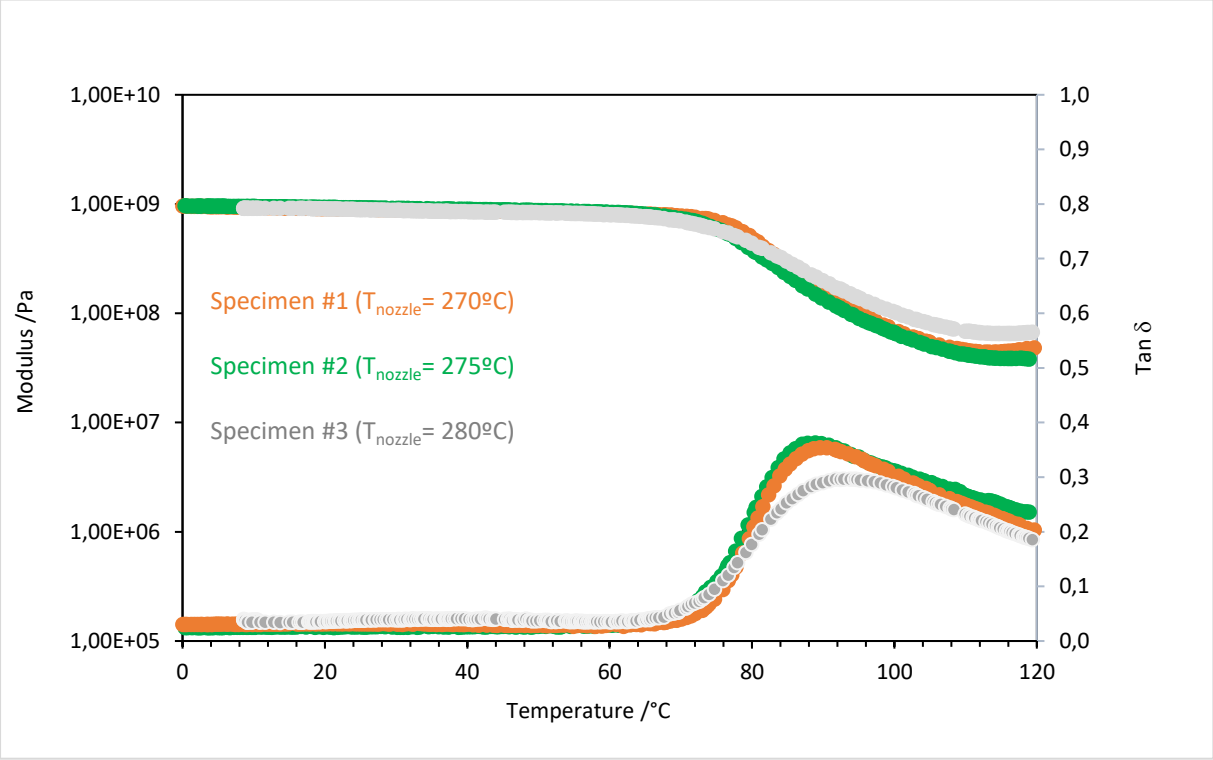

Figure 36: Dynamic mechanical thermal analysis graph obtained for the printed specimen at three different nozzle temperatures.

In this case, it is noticeable that the maximum tan delta of the sample printed at nozzle temperature of 280ºC continues to be lower than those of the samples obtained at nozzle temperatures of 175 and 270º. The difference between the latter is minimal. This result indicates that the samples printed at nozzle temperatures of 175 ºC and 170 ºC present a higher content of amorphous fractions. Furthermore, the T_g value for the specimen printed

with a nozzle at 280 ºC is higher than the other specimens. Once again, the assumptions made above are corroborated.

Printing velocity effect

Figure 37 shows the DMTA results obtained for the three specimens/conditions in which the control parameter is the printing velocity. Table XIII contains the corresponding T_g values and the value of the maximum of tan δ.

Table XIII: Glass transition temperature obtained values for rectilinear printed specimens with the printing velocity being the parameter that is changing.

#SPECIMEN	XYZ CONDITION	**Printing Velocity (mm/s)**	**tanδ $_{max}$**	**T_g (ºC)**
4	C1b	**20**	0.44	**84**
5	C1c	**25**	0.32	**90**
3	C1a	**30**	0.30	**94**

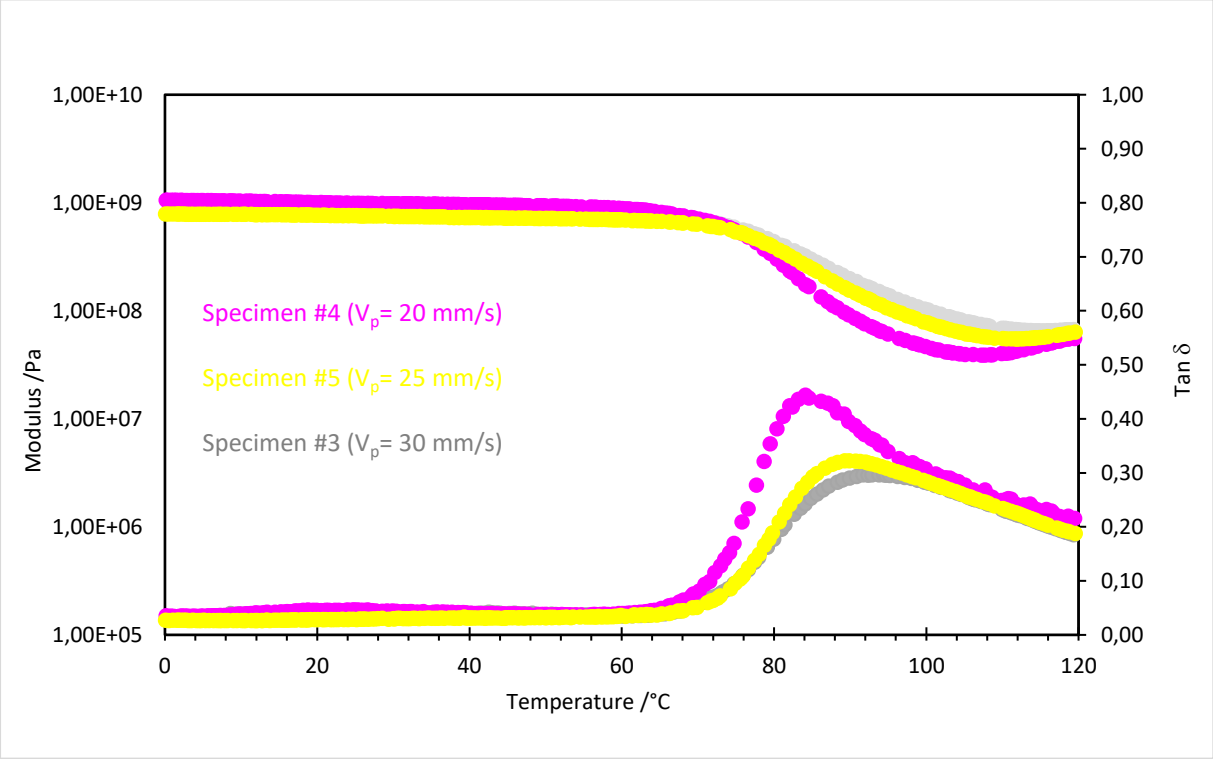

Figure 37: Dynamic mechanical thermal analysis graph obtained for the printed specimen at three different printing velocities.

The results obtained for these samples show a higher value of tan delta for the sample obtained at 20 mm/s, while those obtained at 30 mm/s show the lower. This indicates that the sample obtained at 30 mm/s has a higher crystalline fraction than the one obtained at 20 mm/s. Once more, specimen #3 presents the higher T_g value. These results are in agreement with those obtained by DSC, and the conclusions derived from them can therefore be extended.

In general terms, the results obtained by DMTA confirm the results obtained by DSC. Thus, although a crystallinity gradient along the width of the specimen was detected by DSC, the DMTA results corroborate the general trend observed. That is, the samples in which a higher degree of crystallinity has been detected have given rise to lower maximum tan δ values, indicating a lower overall amorphous phase content, as is the case of specimen/condition 3. Likewise, samples, where a lower degree of crystallinity has been detected by DSC, have

resulted in a significantly higher tan δ maximum, clearly indicating a higher fraction of amorphous phase, as is the case for specimen/condition 7.

IV.iii ***Printed Specimens-CONCENTRICAL fill pattern***

A similar study has been carried out with specimens obtained with a concentric pattern. Figure 38 shows an example of a specimen obtained at each of the seven conditions. In this image, it can be detected that the specimens show colour variation in the wide region of the test bar. The central part of the specimen appears white, while the ends are more transparent.

However, this study will not be presented in this paper because very similar results have been obtained. This happens because, despite using a different pattern, the central area of the specimen (the test area) has been printed in the same way as the previous ones, i.e., in parallel.

Figure 38: Tensile-test printed specimens of seven different printing conditions with the concentrical filling pattern.

IV.ii.d Scanning Electronic Microscope[i]

The analysis of the cross-section of the tensile specimens obtained by 3D printing using SEM permits the visualisation of the real internal structure of the specimens. Thus, for example, the proper distribution of the layers and the good adhesion between them are fundamental factors that can directly affect the final mechanical properties of the printed part.

The following images correspond to the cross-section of the central part of the tensile specimens printed under the seven different conditions. The specimens were cryogenically broken after being kept for 1 hour in liquid nitrogen.

Figure 39 corresponds to the fracture surface of the specimen printed according to A1a printing conditions (#1, 270 ºC nozzle temperature, 100 ºC bed temperature and 30 mm/s printing velocity). In those images, the harmonic sequence in the filament deposition is noticed. The different layers are easily distinguishable, with good adhesion between the filaments. However, the presence of homogeneously distributed holes is also noticeable. Even though these are the printing conditions that have given relatively good results in terms of Young's modulus, the presence of these holes may be the origin of the worst mechanical properties.

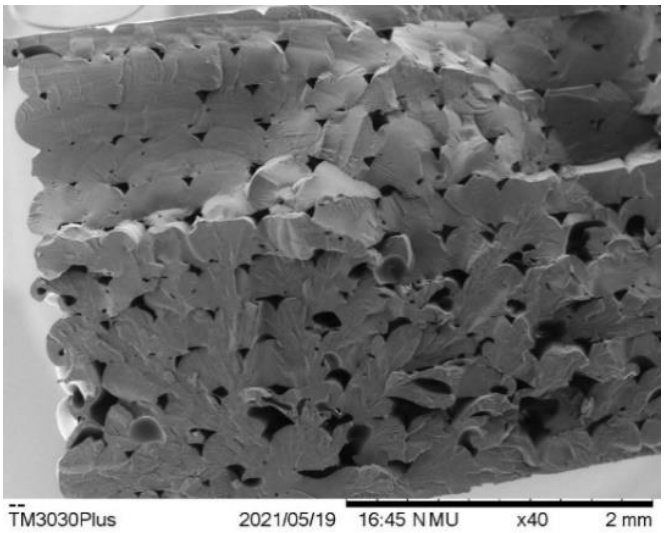

Figure 39: Cross-section of specimen printed at A1a conditions (#1).

,

Figure 40 corresponds to the specimen printed according to B1a printing conditions (#2, 275 ºC nozzle temperature, 100 ºC bed temperature, and 30 mm/s printing velocity). In this image, in addition to the homogeneous distribution of the layers and the correct adhesion between the filaments, the clear distinction between the layers close to the bed (higher crystallinity) and the upper layers (lower crystallinity) is remarkable. The layers close to the bed show a more ordered structure, but with less adhesion surface between filaments. Still, the upper, more amorphous layers show a larger adhesion surface and smaller cavities.

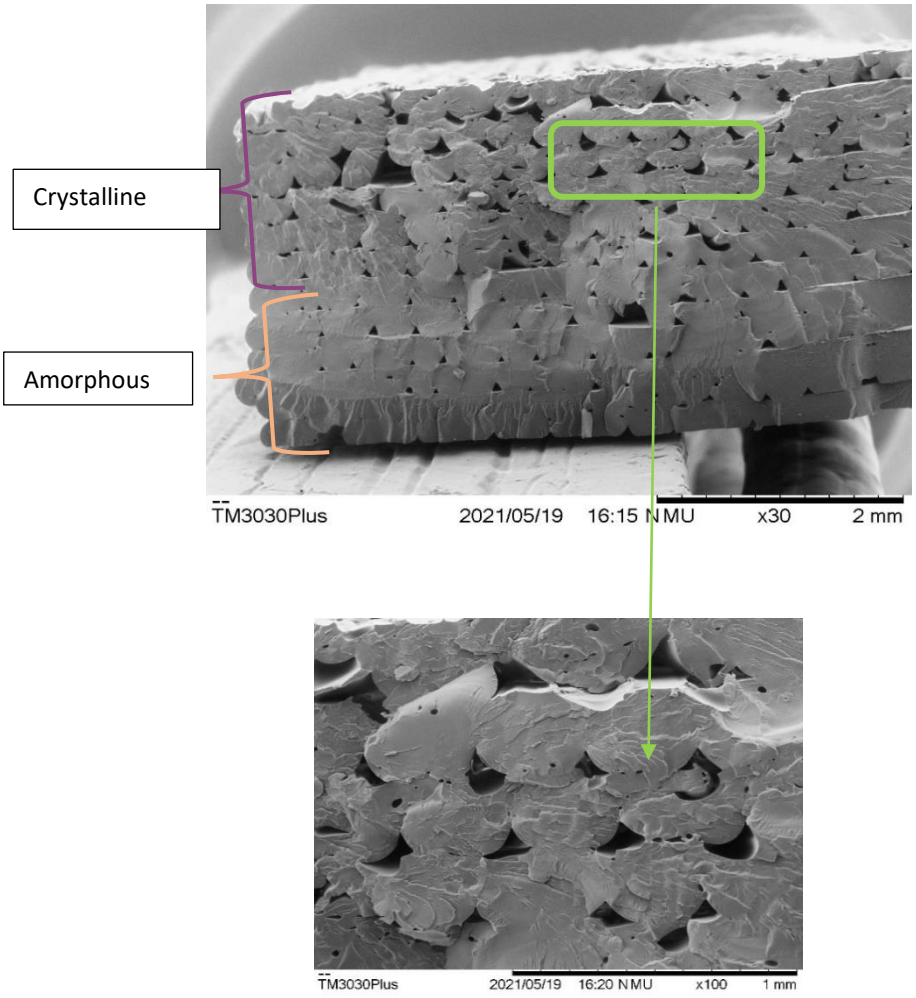

Figure 40: Cross-section of specimen printed at B1a conditions (#2). The distinction between amorphous and crystalline states.

V. OBSERVATIONS

V.I. Warping Effect

It is important to mention the warping effect that some of the printed specimens have presented. The warping is an effect that causes the corners of the printed product to lift and detach from the printer bed due to material shrinkage. During the printing procedure, polymers expand slightly at first and contract as soon as they cool down. When the material contracts too much, it bends up from the bed. It is crucial for the warping to be controlled since it affects the dimensions of the wishing product. One way to prevent warping is to ensure adequate adhesion between the product and the printer bed.

The following Table XIV presents warping measurements for printed tensile-test specimens. The values are in millimetres, and figure 41 shows how the warping is measured. The printed specimen is measured after three days so as to be dimensionally stable [36].

Table VIV: Warping measurements for rectilinearly printed specimens.

#SPECIMEN	XYZ CONDITION	AVERAGE	DEVIATION
1	A1a	1,47	1,12
2	B1a	2,27	0,26
3	C1a	2,08	1,00
4	C1b	1,27	0,85
5	C1c	3,16	1,00
6	C2a	-	-
7	C3a	-	-

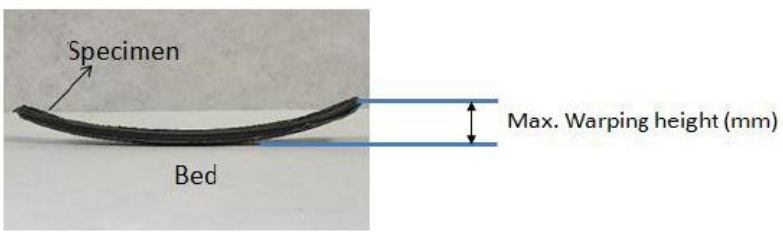

Figure 41: Warping effect measurement.

It is really difficult to draw conclusions on the effect of printing conditions and warping, due to the wide error ranges.

VII. CONCLUSIONS

The study of PET filament performance on the FDM technology was successful. Mechanical properties of the printed products were evaluated and compared with the injected ones. In addition, the effect that some of the printing parameters can have on the mechanical performance of the material was analysed.

The specimens obtained by 3D printing have worse mechanical properties than those obtained by injection moulding. Young's moduli are, in some cases, slightly lower; however, the elongation at break does not reach 5%, while those of the injected specimens exceed 200%. The crystallisation of the PET during printing is one of the causes of these poorer mechanical properties. A crystallisation gradient has been found during 3D printing. The magnitude of the gradient depends on the printing conditions used.

Finally, through the scanning electronic microscope, the organization of the filament deposition was captured. The crystallised regions show an ordered distribution of filaments in the different layers, with larger cavities than in the amorphous regions. The shrinkage of the filament during crystallisation may be responsible for this observation.

The most important part of the whole study is that PET is a good material to be employed in FDM technology. Outlining the possible future of employing polymers in FDM technology, the use of recycled PET should be the focus of further research.

VIII. REFERENCES

(1) Costa, J. P. D. The Environmental Impacts of Plastics and Micro-Plastics Use, Waste and Pollution: EU and National Measures. 76.

(2) Zander, N. E.; Gillan, M.; Burckhard, Z.; Gardea, F. Recycled Polypropylene Blends as Novel 3D Printing Materials. *Addit. Manuf.* **2019**, *25*, 122–130. https://doi.org/10.1016/j.addma.2018.11.009.

(3) Masood, S. H. Advances in Fused Deposition Modeling. In *Comprehensive Materials Processing*; Elsevier, 2014; pp 69–91. https://doi.org/10.1016/B978-0-08-096532-1.01002-5.

(4) Woern, A.; Byard, D.; Oakley, R.; Fiedler, M.; Snabes, S.; Pearce, J. Fused Particle Fabrication 3-D Printing: Recycled Materials' Optimization and Mechanical Properties. *Materials* **2018**, *11* (8), 1413. https://doi.org/10.3390/ma11081413.

(5) Polyethylene Terephthalate Production, Price and Market. Plastics Insight.

(6) The Circular Economy Package: New EU Targets for Recycling | News | European Parliament Https://Www.Europarl.Europa.Eu/News/En/Headlines/Society/20170120STO59356/the-Circular-Economy-Package-New-Eu-Targets-for-Recycling (Accessed 2021 -07 -28).

(7) Transformar nuestro mundo: la Agenda 2030 para el Desarrollo Sostenible. **2030**, 40.

(8) A European Strategy for Plastics in a Circular Economy. EUROPEAN COMMISSION January 16, 2018.

(9) Sinha, V.; Patel, M. R.; Patel, J. V. Pet Waste Management by Chemical Recycling: A Review. *J. Polym. Environ.* **2010**, *18* (1), 8–25. https://doi.org/10.1007/s10924-008-0106-7.

(10) Al-Sabagh, A. M.; Yehia, F. Z.; Eshaq, Gh.; Rabie, A. M.; ElMetwally, A. E. Greener Routes for Recycling of Polyethylene Terephthalate. *Egypt. J. Pet.* **2016**, *25* (1), 53–64. https://doi.org/10.1016/j.ejpe.2015.03.001.

(11) Awaja, F.; Pavel, D. Recycling of PET. *Eur. Polym. J.* **2005**, *41* (7), 1453–1477. https://doi.org/10.1016/j.eurpolymj.2005.02.005.

(12) AlMaadeed, M., Ponnamma, D., Carignano, M. Polymers and Food Packaging. In *Polymer Science and Innovative Applications: Materials, Techniques, and Future Developments*; Elsevier: Cambridge, 2020; p 528.

(13) Bakır, A. A.; Atik, R.; Özerinç, S. Effect of Fused Deposition Modeling Process Parameters on the Mechanical Properties of Recycled Polyethylene Terephthalate Parts. *J. Appl. Polym. Sci.* **2021**, *138* (3), 49709. https://doi.org/10.1002/app.49709.

(14) Pollack, S.; Venkatesh, C.; Neff, M.; Healy, A. V.; Hu, G.; Fuenmayor, E. A.; Lyons, J. G.; Major, I.; Devine, D. M. Polymer-Based Additive Manufacturing: Historical Developments, Process Types and Material Considerations. In *Polymer-Based Additive Manufacturing*; Devine, D. M., Ed.; Springer International Publishing: Cham, 2019; pp 1–22. https://doi.org/10.1007/978-3-030-24532-0_1.

(15) Dizon, J. R. C.; Espera, A. H.; Chen, Q.; Advincula, R. C. Mechanical Characterization of 3D-Printed Polymers. *Addit. Manuf.* **2018**, *20*, 44–67. https://doi.org/10.1016/j.addma.2017.12.002.

(16) Rahim, T. N. A. T.; Abdullah, A. M.; Md Akil, H. Recent Developments in Fused Deposition Modeling-Based 3D Printing of Polymers and Their Composites. *Polym. Rev.* **2019**, *59* (4), 589–624. https://doi.org/10.1080/15583724.2019.1597883.

(17) Mwema, F. M.; Akinlabi, E. T. Basics of Fused Deposition Modelling (FDM). In *Fused Deposition Modeling*; SpringerBriefs in Applied Sciences and Technology; Springer International Publishing: Cham, 2020; pp 1–15. https://doi.org/10.1007/978-3-030-48259-6_1.

(18) Mohamed, O. A.; Masood, S. H.; Bhowmik, J. L. Optimization of Fused Deposition Modeling Process Parameters: A Review of Current Research and Future Prospects. *Adv. Manuf.* **2015**, *3* (1), 42–53. https://doi.org/10.1007/s40436-014-0097-7.

(19) Dolzyk, G.; Jung, S. Tensile and Fatigue Analysis of 3D-Printed Polyethylene Terephthalate Glycol. *J. Fail. Anal. Prev.* **2019**, *19* (2), 511–518. https://doi.org/10.1007/s11668-019-00631-z.

(20) Candal, M. V.; Calafel, I.; Aranburu, N.; Fernández, M.; Gerrica-Echevarria, G.; Santamaría, A.; Müller, A. J. Thermo-Rheological Effects on Successful 3D Printing of Biodegradable Polyesters. *Addit. Manuf.* **2020**, *36*, 101408. https://doi.org/10.1016/j.addma.2020.101408.

(21) Lehrer, J.; Scanlon, M. R. The Development of a Sustainable Technology for 3D Printing Using Recycled Materials. **2017**, 8.

(22) ASTM D638-14, Standard Test Method for Tensile Properties of Plastics,ASTM International, West Conshohocken, PA, 2014.

(23) Zaldivar, R. J.; Witkin, D. B.; McLouth, T.; Patel, D. N.; Schmitt, K.; Nokes, J. P. Influence of Processing and Orientation Print Effects on the Mechanical and Thermal Behavior of 3D-Printed ULTEM® 9085 Material. *Addit. Manuf.* **2017**, *13*, 71–80. https://doi.org/10.1016/j.addma.2016.11.007.

(24) Standard ASTM D1938–19, Standard Test Method for Tear-Propagation Resistance (Trouser Tear) of Plastic Film and Thin Sheeting by a Single-Tear Method, EEUU.

(25) Sichina, W. J. DSC as Problem Solving Tool: Measurement of Percent Crystallinity of Thermoplastics. *Therm. Anal.* 4.

(26) Akhoundi, B.; Behravesh, A. H. Effect of Filling Pattern on the Tensile and Flexural Mechanical Properties of FDM 3D Printed Products. *Exp. Mech.* **2019**, *59* (6), 883–897. https://doi.org/10.1007/s11340-018-00467-y.

(27) Jabarin, S. A. Optical Properties of Thermally Crystallized Poly(Ethylene Terephthalate). *Polym. Eng. Sci.* **1982**, *22* (13), 815–820. https://doi.org/10.1002/pen.760221305.

(28) DemiRel, B.; Yara, A.; Elç, H. Crystallization Behavior of PET Materials. **2011**, 10.

(29) Rana, A. K.; Mitra, B. C.; Banerjee, A. N. Short Jute Fiber-reinforced Polypropylene Composites: Dynamic Mechanical Study. 9.

(30) *Menard, K. P. Dynamic Mechanical Analysis: A Practical Introduction; CRC Press: Boca Raton, Fla, 1999.*

(31) ISO, ISO 527-1:2012 – Plastics – Determination of Tensile Properties – Part1: General Principles, ISO/TC 61/SC 2 Mechanical Behavior, 2012.

(32) Abdul Razak, N. C.; Inuwa, I. M.; Hassan, A.; Samsudin, S. A. Effects of Compatibilizers on Mechanical Properties of PET/PP Blend. *Compos. Interfaces* **2013**, *20* (7), 507–515. https://doi.org/10.1080/15685543.2013.811176.

(33) Ronkay, F.; Czigány, T. Cavity Formation and Stress-Oscillation during the Tensile Test of Injection Molded Specimens Made of PET. *Polym. Bull.* **2006**, *57* (6), 989–998. https://doi.org/10.1007/s00289-006-0670-8.

(34) Davis, C. S.; Hillgartner, K. E.; Han, S. H.; Seppala, J. E. Mechanical Strength of Welding Zones Produced by Polymer Extrusion Additive Manufacturing. *Addit. Manuf.* **2017**, *16*, 162–166. https://doi.org/10.1016/j.addma.2017.06.006.

(35) Sangroniz, L.; van Drongelen, M.; Cardinaels, R.; Santamaria, A.; Peters, G. W. M.; Müller, A. J. Effect of Shear Rate and Pressure on the Crystallization of PP Nanocomposites and PP/PET Polymer Blend Nanocomposites. *Polymer* **2020**, *186*, 121950. https://doi.org/10.1016/j.polymer.2019.121950.

(36) *Unfilled Polyethylene Terephthalate (PET) Https://Polymerdatabase.Com/Commercial%20Polymers/PET.Html (Accessed 2021 -08 -30).*

(37) Torres, N.; Robin, J. J.; Boutevin, B. Study of Thermal and Mechanical Properties of Virgin and Recycled Poly(Ethylene Terephthalate) before and after Injection Molding. *Eur. Polym. J.* **2000**, *36* (10), 2075–2080. https://doi.org/10.1016/S0014-3057(99)00301-8.

(38) Müller, A. J.; Feijoo, J. L.; Alvarez, M. E.; Febles, A. C. The Calorimetric and Mechanical Properties of Virgin and Recycled Poly(Ethylene Terephthalate) from Beverage Bottles: Virgin and Recycled PET From Beverage Bottles. *Polym. Eng. Sci.* **1987**, *27* (11), 796–803. https://doi.org/10.1002/pen.760271105.

(39) Sharma, S. K.; Misra, A. The Effect of Stretching Conditions on Properties of Amorphous Polyethylene Terephthalate Film. *J. Appl. Polym. Sci.* **1987**, *34* (6), 2231–2247. https://doi.org/10.1002/app.1987.070340615.

(40) Salem, D. R. Microstructure Development during Constant-Force Drawing of Poly(Ethylene Terephthalate) FIlm. 11.

(41) Estevez, D.; Sebastián, S. Study of Feasibility of Using Recycled Polyolefins in 3D Printing. 21.